# Blind Deconvolution of Vehicle Inductance Signatures for Travel-Time Estimation

Research

Technical Report Documentation Page

1. Report No. MN/RC-2006-06	2.	3. Recipients Accession No.	
4. Title and Subtitle Blind Deconvolution of Vehicle Inductance Signatures for Travel-Time Estimation		5. Report Date February 2006	
		6.	
7. Author(s) Taek Mu Kwon, Ph.D		8. Performing Organization Report No.	
9. Performing Organization Name and Address University of Minnesota Duluth Department of Electrical and Computer Engineering 1023 Unversity Drive Duluth, Minnesota 55812		10. Project/Task/Work Unit No.	
		11. Contract (C) or Grant (G) No. (c) 81655 (wo) 40	
12. Sponsoring Organization Name and Address Minnesota Department of Transportation 395 John Ireland Boulevard Mail Stop 330 St. Paul, Minnesota 55155		13. Type of Report and Period Covered Final Report	
		14. Sponsoring Agency Code	
15. Supplementary Notes http://www.lrrb.org/PDF/200606.pdf			

16. Abstract (Limit: 200 words)

     Travel-time data provides vital information for traffic monitoring, management, and planning. The objective of this research was to develop a new computational approach that could accurately measure travel time from two sets of spatially separated loop detectors using re-identification of vehicle inductance signatures generated by the loops. Although measuring travel time using loop inductance signatures is not new, all past approaches essentially relied on pattern matching of raw inductance waveforms without restoring the loss of detailed features caused by a large detection zone of inductive loops. The main effort in this research was to develop a new computational algorithm that restores the lost details from the raw inductance waveforms by modeling the output of loop detectors as a convolution of the original vehicle signature and the loop system function. This restoration problem was formulated as a blind deconvolution problem since we know neither the impulse response of the loop detectors, nor the original vehicle signature. To solve this blind problem, two basic blind deconvolution approaches were used, Godard deconvolution and constrained least squares. Experimental results showed that both methods performed well and significantly exposed the original signature information with unique vehicle characteristics.

17. Document Analysis/Descriptors Travel time, inductance signature, blind deconvolution, FFT		18. Availability Statement No restrictions. Document available from: National Technical Information Services, Springfield, Virginia 22161	
19. Security Class (this report) Unclassified	20. Security Class (this page) Unclassified	21. No. of Pages 64	22. Price

Blind Deconvolution of Vehicle Inductance Signatures for Travel-Time Estimation

Final Report

Prepared by:
Taek Mu Kwon, Ph.D.
Department of Electrical and Computer Engineering
University of Minnesota, Duluth

February 2006

ACKNOWLEDGEMENTS

TABLE OF CONTENTS

LIST OF TABLES

LIST OF FIGURES

EXECUTIVE SUMMARY

Travel-time data provides vital information for traffic monitoring, management, and planning. The objective of this research was to develop a new computational approach that could accurately measure travel time from two sets of spatially separated loop detectors using re-identification of vehicle inductance signatures generated by the loops. Although measuring travel time using loop inductance signatures is not new, all past approaches essentially relied on pattern matching of raw inductance waveforms without restoring the loss of detailed features caused by a large detection zone of inductive loops. The main effort in this research was to develop a new computational algorithm that restores the lost details from the raw inductance waveforms by modeling the output of loop detectors as a convolution of the original vehicle signature and the loop system function. This restoration problem was formulated as a blind deconvolution problem since we know neither the impulse response of the loop detectors, nor the original vehicle signature. To solve this blind problem, two basic blind deconvolution approaches were used. The first approach estimates the loop system function using a speed estimate obtained from the inductance waveform. The estimated loop system function is then used in constructing a Constrained Least Squares (CLS) inverse filter that restores the lost information. The second approach used is an adaptive iterative method referred to as the Godard blind deconvolution. This approach finds the inverse filter through repeated iterations without the knowledge of the system function. However, it was found that the iteration converges to a better solution when the initial condition was set using a CLS filter estimate. Experimental results showed that both methods performed well and significantly exposed the original signature information with unique vehicle characteristics. A simple feature extraction technique along with sum of difference coefficients was implemented to test the re-identification rates. The test runs showed that vehicle re-identification rates after deconvolution are substantially higher (near 89%) than those before deconvolution (60%). The results obtained are encouraging and suggest that blind deconvolution is an effective technique that can be used for extracting the lost information from the loop inductance outputs.

1. INTRODUCTION

1.1 Objective

Travel-time measurement in today's complex roadway network provides vital information for traffic monitoring, management, and planning. It serves traffic engineers as an important tool for evaluating the efficacy of traffic networks and for measuring the performance of traffic management strategies. It is also a critically important parameter for developing real-time route guidance systems. The effectiveness of such systems depends on reliable and timely measurements of travel time.

Direct measurement of travel time by driving the route perhaps produces the most accurate travel time of the route and is frequently used to verify the predicted travel time. On the other hand, this approach is impractical as it requires many vehicles and human resources for repetitive and frequent measurements. The approach proposed in this research is to estimate the travel time using signal analysis of inductance signatures obtained from the existing inductive loop detectors (ILD). More specifically, the travel time is obtained from the arrival-time differences at the measuring pair of stations through identification and re-identification of vehicles by inductance signature analysis. This approach is cost-effective since many highways and arterials already have large installed bases of ILD, and can produce direct measurements of travel time equivalent to driving the route. Hence, several researchers have attempted to develop real-time travel-time measurement techniques based on inductance signatures in the past. However, prior approaches have mainly focused on developing pattern recognition algorithms directly utilizing the raw inductance waveforms. On the other hand, the inductance outputs of ILD are inductance changes scanned by the large detection zone of loops and do not contain detailed features due to the moving average effect. Unfortunately, none of the prior approaches attempted to restore the lost signature information from the moving average effect and resulted in poor re-identification performance. Therefore, the objective of this research is to develop a new signal processing algorithm that restores the loss of the details in the inductance waveforms before using the inductance signatures for pattern recognition. As a basic methodology, the ILD output is modeled as a convolution of the true inductance signature and the loop system function. We attempt to restore the lost

details through development of an inverse filter. This type of signal restoration techniques is referred to as deconvolution and is one of the classical areas of signal processing. Since we neither have information on the loop system function nor the true inductance signature, this problem is referred to as a blind problem. Therefore, a class of algorithms referred to as a blind deconvolution (Haykin, 2000) is investigated and used as the basic methodology for the inductance signature restoration in this research.

1.2 Related Works On Travel Time

Travel time may be obtained in a number of ways. They can be measured directly using probe vehicles or by location identification technologies (e.g., automatic vehicle location (AVL) by GPS and automatic vehicle identification (AVI) tags), or estimated indirectly from the volume and occupancy of traditional traffic data. However, each method has its own limitations and drawbacks in real-world traffic application, and new efficient approaches are still being sought by many researchers.

Estimating speeds using volume and occupancy relationships of loop data and converting them into travel time has been proposed by numerous researchers (Dailey, 1999; Mikhalkin, 1972; Pushkar, 1994; Coifman, 2000), but the limitation in their accuracy under delayed conditions (e.g., incidents and congestions) has been widely observed. Another problem with these methods is that it requires average vehicle length which is not obtainable from the volume and occupancy data itself and changes moment to moment.

Recently, measurements of travel time have been increasingly viewed as an important issue in traffic monitoring and management. As a result, several pioneering research projects have been proposed and are under way. In the California PATH program, researchers (Tam 1999/2000, Yim et al. 2000) have been studying the use of cell phones and GPS units to probe the location of vehicles for travel time estimation. Others (Tam 1999/2000) proposed the use of video-based signature analysis in which vehicle tracking is accomplished using the analysis of video images. Use of a real-time laser-based detection system for speed from which it is converted to travel time was another method proposed (Tam 1999/2000).

In another direction, researchers began to investigate utilization of inductance changes in ILDs. The data obtained from the conventional ILDs is in a form of digital logic (on/off) indicating the presence of a vehicle over the loop. However, new generation of ILDs began to provide the waveforms of inductance changes of the loop. The shape of this inductance waveform depends on various factors such as the length of the vehicle, speed of the vehicle, the material with which the vehicle is made, the height of the vehicle body from the road surface, etc. Since the ILD waveforms can provide considerable amount of information about the vehicle, numerous new applications of loop detectors began to emerge, such as vehicle classification and single-loop speed measurements (Sun & Ritchie, 1999, Sun, 2000). Sun proposed two different classification methods that utilize inductance waveforms to classify vehicles into seven predefined vehicle classes (Sun, 2000). The first method uses a Self-Organizing Feature Map (SOFM), which is a well known artificial neural network approach that has been used in pattern classifications. The second method uses a heuristic discriminant algorithm to classify the vehicles. The inputs to this algorithm are feature vectors obtained by processing the ILD waveforms. The feature vectors include the length, signature variance, skewness, kurtosis, and Discrete Fourier Transform (DFT) coefficients (Sun 2000). Another study by Sun and Ritchie (1999) uses single ILD signatures for the estimation of individual vehicle speed. This method makes use of the fact that the speed of a vehicle is correlated to the slew rate of the ILD waveform where the slew rate is the rate of change in inductance. The algorithm calculates the slew rate by extracting the leading and trailing edges of the inductance waveform by finding the local maxima. The speed is then estimated using a linear regression method. These approaches are still in initial research states, and further study is needed to increase the accuracy.

As an alternative to the above approaches, vehicle travel time can also be estimated by using a pair of ILD stations (upstream and downstream station). In this approach, the vehicle arrival times at two stations are tracked, and the travel time is obtained from the difference of the arrival times. However, this approach requires re-identification of the same vehicle at the second loop by matching the vehicle signature. The problem of vehicle re-identification can be tackled in several ways. One algorithm proposed by Sun et al. identifies the upstream origin of the vehicle based on either a

heuristic method or a probabilistic neural network (PNN) method (Sun et al. 2002) without specific features being extracted. Another methodology is to extract specific features of the inductance signatures generated by each vehicle and then use them for re-identification. In this approach it is important to extract detailed or particular features from the signatures that expose the uniqueness of each vehicle to achieve a high re-identification rate.

In the prior approaches mentioned above, inductance outputs of ILD have been directly used for vehicle pattern identification. Such approaches have an inherent limitation in the identification rates, since the inductance outputs are actually generated as a moving average of inductance changes with the window size determined by the loop detection area (typically 6 x 6 feet). A new approach that this research pursued is to remove the moving average effect from the raw inductance outputs using a class of techniques called blind deconvolution (also called blind separation for multiple inputs) before applying the pattern recognition techniques. In essence, this process restores the detailed inductance information lost from the convolution process and exposes more uniqueness of each signature. This uniqueness of signatures helps to improve the re-identification rate from which more accurate travel time is measured.

2. THEORETICAL BACKGROUND

2.1 Inductive Waveform

Inductive loop detectors (ILD) consist of one or more turns of loop wires embedded in the pavement and control electronics. The loop wires are excited by an alternating current (AC) signal ranging from 10 KHz to 200 KHz and act as a resonance circuit that operates on the principle of resonance caused by the electromagnetic inductance and capacitance. The loop wires function as an inductive element, and the capacitance is provided by the capacitors embedded in the detector card. The control electronics constantly send AC to the loop circuit to maintain a constant level of inductance at the loop sensing zone. As a vehicle passes over the loop, the magnetic field formed by the loop wires induces eddy currents on the metal surface of the vehicle. The eddy currents then produce a magnetic field in an opposite direction to the magnetic field generated by the loop, and cancel out some portion of the loop's magnetic field. This cancellation of the magnetic fields reduces inductance of the circuit formed by the loop wires and results in reduction of the inductance in the resonance circuit. The resonance frequency in relation to the inductance and capacitance follows the general resonance principle, i.e.,

$$\text{Resonance frequency} = \frac{1}{2 \times \pi \times \sqrt{L \times C}} \tag{1}$$

where L is the inductance and C is the capacitance of the loop circuit. Notice that, when the inductance is decreased, the resonance frequency is increased. Therefore, when a vehicle is present over the loop, the inductance is decreased and the resonance frequency is increased. This frequency increase is detected by the control electronics, typically by zero-cross counting. In some detector cards, this frequency increase is computed back to inductance changes. The change in inductance due to the presence of a vehicle is recorded at a small time-interval and becomes the inductance waveform. This waveform is referred to as the *vehicle inductive waveform* or *inductance signature* and has been the main source of vehicle re-identification using loop detectors.

Figure 2.1 shows an inductive waveform of a typical two-axle passenger car. The horizontal axis is a recording of data points at 10 milliseconds interval and the vertical axis shows the inductance changes. Notice that the inductance was decreased when a

vehicle was present over the loop. In the past approaches, raw inductance waveforms such as shown in Figure 2.1 have been directly used to extract vehicle features (Sun, 2000). Since most ILD sensing zones (typically 7'x7' in a 6'x6' loop) are relatively large in reference to the vehicle size, the inductance outputs are not the detailed features of the vehicle but a moving average of the inductance changes caused by the overlapped area between the loop-sensing zone and the vehicle (convolution). Consequently, many details of the vehicle features are already lost by this moving average effect. This is evident from the common shape of the inductance waveforms from two-axle vehicles in which most of them have one peak in the middle with monotonic decrease in both sides of the curve as shown in Figure 2.1. A more accurate representation of the inductance signature of two-axle vehicles should have been at least two valleys corresponding to the two axles. Such information is lost due to the large size of the ILD sensing zone.

Vehicle Signature
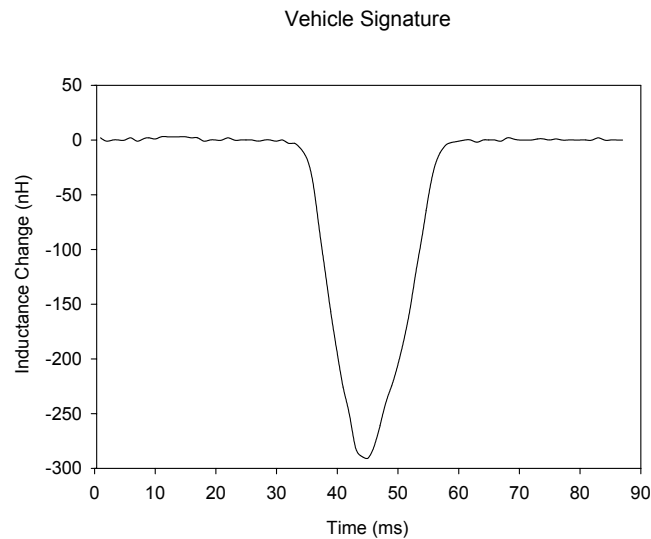
Figure 2.1 Inductance waveform of a typical passenger vehicle. Horizontal axis intervals are in 10 milliseconds.

2.2 Blind Deconvolution

In system theory, the output of a linear system is commonly modeled as a convolution of the input and the system function. In a similar manner, the inductance output of an ILD is modeled as a convolution between the inductance signature of the vehicle and the loop characteristic function in this research. More specifically, the ILD system function is similar to a moving average filter from which the vehicle inductance features are convolved. In this system setting, the inputs are the ideal inductance

6

signature that we wish to find from the observed output of the convolution system without knowing the system function. This type of problem is referred to as a blind problem, and a class of techniques used to solve them is referred to as *blind deconvolution* (Haykin, 2000).

The objective of blind deconvolution in the feature extraction process is to find an inverse system such that the estimates of the vehicle signal are recovered, i.e., $y \approx f$ as shown in Figure 2.2. Since we know neither the vehicle signal nor the loop conditions from the observed inductance output, this process is a blind operation.
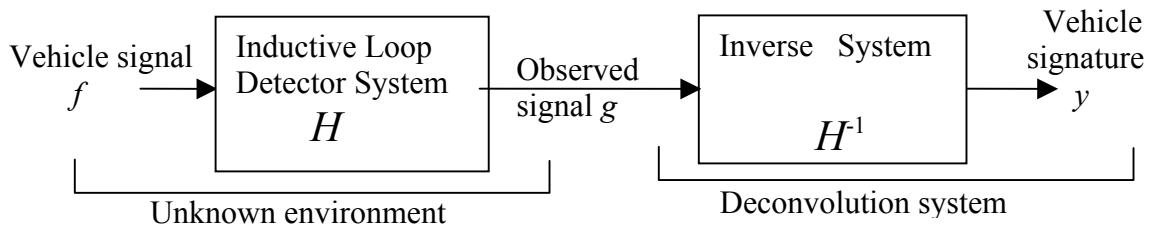
Figure 2.2: Block diagram illustrating convolution and deconvolution process for vehicle signature extraction.

The techniques used for blind deconvolution are similar to the ones used for blind channel-equalization in communication. The need for channel equalization arises from the fact that, during signal communication, the channel through which the signal is propagated usually distorts the original signal. In channel-equalization, the distortion by the channel is cancelled from the received signal using channel equalization (interference cancellation) techniques. One of the earliest developed techniques for blind channel equalization is the decision-directed (DD) algorithm developed by Lucky in 1966 at the Bell Laboratory (Lucky, 1966). This method utilizes a decision-directed mode of operation on the least-mean-squares algorithm. The Sato algorithm was developed in 1975 motivated by the fact that the DD algorithm failed to readapt to a newly connected channel (Sato, 1975). Godard made another important contribution when he introduced a dispersion cost function that ensures existence of local minima (Godard, 1980). Many of the constant-modulus (CM) blind deconvolution techniques used today have their roots in the Godard algorithm.

One way to achieve blind deconvolution is by unsupervised adaptive filtering. Adaptive filtering is a form of recursive filtering in which the filter parameters are adjusted until the desired output is obtained. Adaptive filtering is termed as unsupervised when the filter parameters are adjusted without having the desired response of the filter. However, even for the unsupervised, the filter parameters are adjusted according to a set of rules, which allows the filter to calculate a desirable input to output mapping. There are three fundamental approaches to unsupervised adaptive filtering:

1. Bussgang Statistics
2. Higher order statistics
3. Information-Theoretic models

A Bussgang process has the property that its autocorrelation function is equal to the cross-correlation between the process and the output of a zero-memory non-linearity produced by that process (Haykin, 2000). Hence, for a Bussgang process the output follows a condition given by:

$$E[y(t)y(t-k)] \approx E[y(t)\, g(y(t-k))] \tag{2}$$

where $g(\bullet)$ represents a non-linearity. Unsupervised adaptive filters that satisfy this condition are classified as Bussgang algorithms. These include the DD algorithm, Sato algorithm, and constant-modulus algorithms (CMA) (Haykin, 2000). A block diagram of an unsupervised adaptive filter of the Bussgang type is shown in Figure 2.3 (Haykin, 2000). The input $x(t)$ to the filtering system is the distorted signal received or observed. The aim of this adaptive filtering is to design a finite impulse response (FIR) filter that can recover the original uncorrupted signal from $x(t)$ without knowing the transfer function of the distorting system. The parameters of the FIR filter are recursively adjusted until the output of the non-linearity gives a close approximation to the FIR filter output $y(t)$. When the adaptation process converges, i.e. the error $e(t)$ is close to zero, the FIR filter approximates the inverse of the transfer function that has distorted the output.
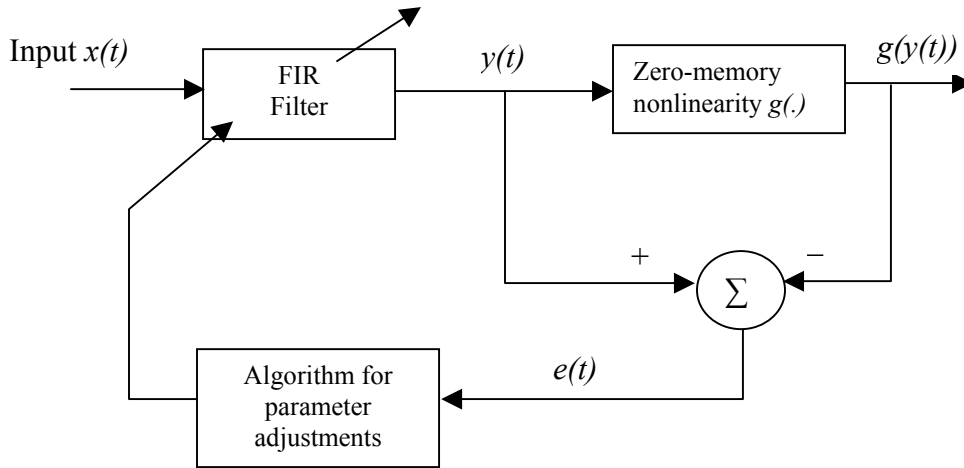
Figure 2.3: Adaptation using Bussgang type algorithms

Bussgang algorithms have been widely used for blind equalization of noisy communication channels and improved over the years. Nowlan and Hinton developed a soft decision-directed least-mean-squares algorithm that converges in channels where the conventional DD algorithm fails to converge (Nowlan and Hinton, 1993). Another work by Weerackody et al. uses the Sato algorithm and the Godard algorithm for initial convergence but switches to the DD algorithm when the error has a very small value (Weerackody et al., 1994). This is because both the Sato algorithm and the Godard algorithm have a slow convergence rate. Among many Bussgang algorithms, CMA has been the most studied and implemented algorithm for blind equalization in the 1990s (Johnson et al., 1998). The choice of the algorithm to use depends on the communication systems used, the convergence rate required, and the acceptable residual error after convergence (Lee & Cheun, 1999).

The mentioned approaches were developed to recover digital communication signals and worked well for phase modulation distortions, but failed to perform well when they were applied to impulsive signals (Mathis & Douglas, 1999). Mathis & Douglas provided a theoretical and analytical explanation as to why the conventional Bussgang algorithms are unsuitable for impulsive signals (Mathis & Douglas, 1999).

Their work discusses a modified Sato algorithm, which can be used for impulsive signals such as acoustic signals in seismic and audio signal processing. Nokas et al. proposed to use blind deconvolution to deconvolve the speech signals that contain the impulse response of the surrounding and the impulse response of the transducer (Nokas et al., 1998). In their approach the CMA algorithm was used for adaptive deconvolution, and a higher order statistical blind deconvolution method was used to estimate the impulse response of the room.

The second type of blind deconvolution approaches makes explicit use of the higher order statistics of the observed signal. The higher-order statistics (HOS) of a stationary process are described in terms of cumulants (generalization of autocorrelation function) and their Fourier transforms known as polyspectra (generalization of power spectrum). The HOS approaches attempt to estimate the impulse response $h[n]$ of the distorting system (system identification) by using information hidden in the cumulants (Olofosson, 1996). Higher order (>2) cumulants contain not only the amplitude but also phase information of the unknown system (Feng & Chi, 1999) as opposed to an autocorrelation function which does not preserve the phase information of the signal. Another added advantage of using higher order cumulants is that they are insensitive to Gaussian noise. However, higher order statistics are mainly applicable when dealing with non-Gaussian processes (Feng & Chi, 1999). Fortunately, many real-world applications are truly non-Gaussian (Feng & Chi, 1999). Another important factor that has to be considered while estimating the impulse response, $h[n]$, is whether the system is a minimum phase system or not. Other methods such as the prediction error method (PEM) are known to have problems in identifying non-minimum phase systems (Olofosson, 1996). However, higher order cumulant approaches can be used in estimating impulse response for a non-minimum phase system.

High order cumulants-based techniques can be classified into two categories: non-parametric and parametric methods. The non-parametric methods are Fourier based and work in the frequency domain, but are not popularly used (Mendel, 1991). The parametric methods first estimate the parameters of the system generating the output and then use it to compute the polyspectrum (Feng & Chi, 1999). These methods provide

results with higher resolution and lower variance and hence are preferred over the non-parametric ones (Zheng et al., 1991). Most parametric methods use second order, third order, fourth order or a combination of these ordered cumulants. Olofsson and others (Olofsson et al., 1996) compared the results obtained from the higher order cumulant method with the classical PEM along with two other methods (Nowlan & Hinton, 1993). They also presented the results to illustrate their capability to identify minimum and non-minimum-phase systems. Another study by Feng and Chi proposed an inverse filter criterion for optimum inverse filter design using joint cumulants (Feng and Chi, 1999). This method attempts to find an optimum inverse filter *v(n)* by maximizing the cost function given by:

$$J_{r,m}(v(n)) = \frac{|C_m\{e(n)\}|^r}{|C_r\{e(n)\}|^m} \tag{3}$$

where r is even, $m > r \geq 2$, and $C_m\{e(n)\}$ and $C_r\{e(n)\}$ denote the *m*-th order and *r*-th order cumulants of *e(n)*, respectively (Feng & Chi, 1999). This method is actually based on the criteria for blind deconvolution of non-minimum phase channels, which were proposed by Shalvi and Weinstein for communication channels (Shalvi and Weinstein, 1990). A similar algorithm based on third and fourth order cumulants was proposed by Zheng et al. for blind deconvolution and identification of non-minimum phase systems (Zheng et al., 1991). However, this algorithm makes use of only the diagonal cumulants, which makes it simpler. It reduces the problem of blind deconvolution to solving a set of linear equations.

Another class of techniques used for blind deconvolution is based on information-theoretic models. These techniques utilize the concepts rooted in Shannon's information theory, which include entropy, mutual information, and Kullback-Leibler divergence (Haykin, 2000). The entropy of a process is defined as the amount of information in that process. It is simply a measure of self-information (information about the process itself). Another important notion is that of mutual information. Mutual information refers to the information contained in one process about another process. Let the vector *y* denote the output of a system in response of input vector *x*. Mutual information, denoted by *I(X,Y),* between the input and output vectors is defined as the difference between the entropy of *x*, denoted by *h(X),* and the conditional entropy of *x* given *y*, denoted by *h(X|Y),* i.e.,

$$I(X;Y) = h(X) - h(X \mid Y)$$

$$= -\int_{-\infty}^{\infty} \int_{-\infty}^{\infty} f(x,y) \log\left(\frac{f(x \mid y)}{f(x)}\right) \tag{4}$$

where $f(.)$ denotes probability density functions. From Eq. (4), the mutual information is interpreted as the information contained in one process minus the information contained in the process when the other process is known (Gray, 1990). More specifically, mutual information represents the difference between the entropy before observing the system output and the conditional entropy about the input after observing the system. This difference contains the unknown system information and is used as a criterion for blind operations. Based on this concept, Bell and Sejonowski (Bell, 1995) devised maximization of the differential entropy for blind source separation (Bell and Sejonowski, 1995). Another common approach is to view the mutual information $I(X,Y)$ as the Kullback-Leibler divergence between the joint density function $f(x,y)$ and the product of marginal probability density functions $f(x)$ and $f(y)$ (Amari et al., 1996). Most of these algorithms were developed as a blind source separation solution, but can be turned into a blind deconvolution solution by constructing it as a maximization of the entropy $H(y)$ of a non-linearly transformed signal $y = g(x)$ where g is some function and x is the input (Haykin, 2000).

The three classes, i.e., Bussgang Statistics, higher order statistics, and information theoretic models are the main techniques used for blind deconvolution. As noted from the diverse methods introduced in this section, a vast number of blind-deconvolution algorithms have been developed over the past 30 years. Therefore, once the ILD inductance outputs are modeled as a convolution system, a huge number of algorithms exist for restoring the features of true inductive signatures.

3. DECONVOLUTION AND BLIND-DECONVOLUTION MODELS FOR VEHICLE RE-IDENTIFICATION

3.1 Convolution Model of Inductive Loop Detector

From a system point of view, the inductance signature of a vehicle can be modeled as a convolved signal between the vehicle signal (inductance-change characteristic) and the loop system function (see Figure 2.2). The system function of an ILD is essentially similar to a moving average filter since the loop typically covers an area (the detection zone of a 6'x6' loop is about 7'x7') in which the vehicle is present. Consequently, many details of the vehicle characteristics are lost as discussed in Section 2.1. The objective of deconvolution is then to restore or extract the original vehicle signature from the convolved output of an ILD. First, an appropriate ILD system model must be established in order to construct the restoration problem as a deconvolution problem. As in any signal system, noise would be contained in the output. Since the system output is produced by an electrical system, the noise can be modeled as Gaussian random noise. Including the additive noise effect, this research proposes to model the output of an ILD system as follows:

$$g = Hf + n \qquad (5)$$

where g, f and n are M-dimensional column vectors that denote the ILD output, the true vehicle signature, and the Gaussian random noise, respectively. The column vectors are:

$$g = \begin{pmatrix} g(0) \\ g(1) \\ \vdots \\ g(M-1) \end{pmatrix}, \qquad (6)$$

$$f = \begin{pmatrix} f(0) \\ f(1) \\ \vdots \\ f(M-1) \end{pmatrix}, \qquad (7)$$

13

and

$$n = \begin{pmatrix} n(0) \\ n(1) \\ \vdots \\ n(M-1) \end{pmatrix}.$$

(8)

Each component of the column vectors in Eqs. (6), (7), and (8) corresponds to the digital sequence of the original analog values. The ILD system, H, is an M x M matrix and expressed by a circular shift of the rows to the right, i.e.,

$$H = \begin{pmatrix} h(0) & h(M-1) & h(M-2) & \dots & h(1) \\ h(1) & h(0) & h(M-1) & \dots & h(2) \\ h(2) & h(1) & h(0) & \dots & h(3) \\ \vdots & \vdots & \vdots & & \vdots \\ h(M-1) & h(M-2) & h(M-3) & \dots & h(0) \end{pmatrix}$$

(9)

A square matrix in which each row is a circular shift of the preceding row and the first row is a circular shift of the last row, is called a circulant matrix and commonly used for modeling convolution (Gonzalez & Woods, 1993). It is also called a channel convolution matrix (Haykin, 2000).

3.2 Deconvolution using CLS Wiener filter

The only known and available value from our base model Eq. (5) is the ILD system output g. One way of solving this system equation is by estimating the circulant matrix H using an impulse response of the ILD system. A number of methods for estimating impulse response will be discussed in Section 3.4. Assuming that the system matrix H can be estimated, our objective is now shifted to finding f using the observed vector g given H. For solving Eq. (5), a cost function J that minimizes the error is constructed using least squares, i.e.,

$$J(f) = \frac{1}{2} \| g - H * f \|^2$$

(10)

14

Eq. (10) is often referred to as a *least-squares* cost function (Gonzalez & Woods, 1993). The task is then reduced to finding f that minimizes the cost function. The minimum can be found by differentiating J with respect to f and by setting the resulting vector equal to a zero vector, i.e.,

$$-H^T(g - Hf) = 0 \, ,$$
(11)

Next, solving for f yields,

$$\hat{f} = \frac{H^T g}{(H^T H)^{-1}}$$
(12)

The least-squares solution derived in Eq. (12) tends to be unstable when H contains singular values (Gonzalez & Woods, 1993). A more stable approach called regularization was thus used in this study. This approach has the following cost function:

$$J(f) = \frac{1}{2}(\| g - H\hat{f} \|^2 - \| n \|^2) + \frac{1}{2}\alpha \| Qf \|^2$$
(13)

where α is called a regularization parameter and Q is a linear operator that works as a stabilizer. Since the second term in Eq. (13) works as a constraint, this approach is often referred to as a constrained least squares (CLS) filter and has been widely used for solving linear system functions (Gonzalez & Woods, 1993). However, when the observed output g contains impulsive noise, the solution of Eq. (13) tends to be distorted. Minimizing this distortion was extensively studied by Zervakis & Kwon using robust CLS functinals and they demonstrated its applications for restoring corrupted images (Zervakis & Kwon,1993). Such sophisticated treatments are not needed in this case due to the absence of impulsive noise.

Since Eq. (13) is a quadratic function, the true signature f that minimizes the cost function is obtained from the first derivative, i.e., by computing,

$$\frac{\partial J(f)}{\partial f} = 0$$
(14)

Solving f in Eq. (14) gives the estimate of the original vehicle signature $\hat{f}$ as,

$$\hat{f} = \frac{H^T g}{H^T H + \alpha Q^{*T} Q} \, .$$
(15)

where Q^* denotes complex conjugate of Q. The linear operator Q is usually implemented as a high pass filter. This type of inverse filter has been used in signal restoration. In Eq. (15), H is the loop system function that is estimated from the inductance waveform, and the matrix computation is done in the frequency domain using Fast Fourier Transform (FFT).

3.3 Vehicle Signature Restoration Using Godard Blind Deconvolution

In communication channels, impulse response is easily estimated using pilot impulse signals during the initial learning phase. In an ILD system, since the impulse input must be a form of physical system that moves over the loop, it is not easy to obtain. More specifically, it is difficult to generate an impulse input since we do not know what constitutes the impulse system input of the loop system. Thus, the problem of finding the vehicle signature is a true blind problem, and a blind deconvolution algorithm is needed for the solution.

Figure 3.1 illustrates the Godard blind deconvolution process that does not require the knowledge of H. In this case, the inverse filter W is selected as a rough initial estimate (an inverse of square or Gaussian function is a good estimate), and then the iteration is repeated until the filter parameter converges or the error is close to zero. This classical deconvolution method is used as the basic approach in this study.
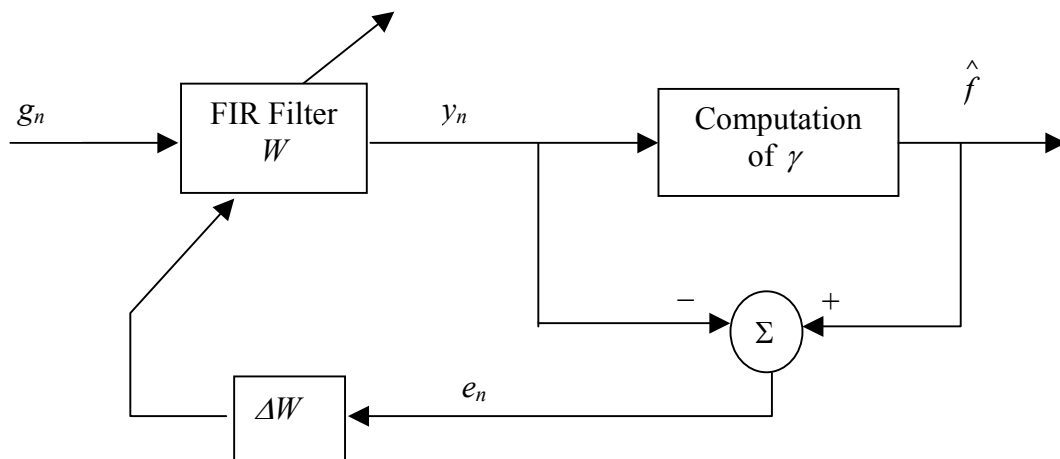
Figure 3.1: Godard Deconvolution

From Figure 3.1, an estimate of the true signature denoted by y is computed as the convolution of the ILD output g with an estimated inverse system W with M parameters, i.e.,

$$y = gW \tag{16}$$

where y and g are both M-dimensional column vectors, and W is an (M x M) block circulant matrix. Using the statistical properties of y, the nonlinearity γ in the Godard blind deconvolution, is chosen as,

$$\gamma = \frac{E[|y_n|^4]}{E[|y_n|^2]} \tag{17}$$

or equivalently,

$$\gamma = \frac{E[|y_n|^4]}{\sigma_y^2} \tag{18}$$

The Godard criterion is then written as

$$J = \frac{1}{4} E\left\{(|y_n|^2 - \gamma)^2\right\} \tag{19}$$

The amount of error ΔW is computed by minimizing this criterion and is obtained as:

$$\Delta W = y_n(\gamma - y_n^2) \qquad . \tag{20}$$

The inverse filter coefficients for the new iteration are then calculated as follows,

$$W(k) = W(k) + \eta \Delta W g(k - M - 1) \tag{21}$$

where η is an iteration rate that is selected depending on the statistical condition of output y_n to make the system converge. When the iteration converges, the resulting inverse filter W becomes close to the inverse of the ILD system. It is then used to get the final output by convolving it with the ILD output to retrieve the true signature, i.e.,

$$\hat{f} = gW \tag{22}$$

Notice that the final estimate only involves the knowledge of the observed vehicle waveform. Since it is computed without the knowledge of the system function, this operation is referred to as a blind operation. For actual implementation, the algorithm is implemented using FFT for efficient computation. The final DFT output is then converted back into discrete time domain.

3.4 ILD Impulse Response Modeling

As discussed in the previous sections, we do not need to know the precise impulse response of the ILD system to successfully extract the vehicle signatures for the Godard deconvolution, but a reasonable estimate that can be used as a starting point of the blind deconvolution iteration. For the CLS filtering, a precise estimate of impulse response is needed. This section discusses how to obtain the initial estimates.

The shape of the loop impulse response can be modeled by considering the amount of flux produced by the loop over its area of 6x6 ft. The magnetic flux produced by the loop increases from the edge, reaches a peak plateau in the middle, and then decreases towards the other edge of the loop. The duration for which a vehicle is induced with eddy currents by the loop flux is the time needed for a vehicle to pass over the loop. This duration depends on the speed of the vehicle as well as the length of the vehicle. Thus, the length of the loop impulse response should be modeled for each vehicle as a function of its speed and the time it will take to pass over the 6 ft loop. To achieve this it is necessary to estimate the speed of the vehicle from a single loop signature. The length of the signature gives the time needed for the vehicle to cover a distance of 6 ft in addition to the vehicle's length itself. Using estimated lengths of vehicles, the vehicle speed is estimated using the following relation,

$$Speed = \frac{(6+length) \times 0.6818}{sig\_len} \tag{23}$$

where, *Speed* = estimated vehicle speed in miles per hour

length = estimated length of the vehicle

sig_len = length of the inductance signature

In this formulation, an estimate of vehicle length is needed. This problem could be solved using the basic features of the inductance waveforms. The number of peaks in the signature in general tells the type of the vehicle from which the estimate of vehicle length can be drawn. Table 3.1 summarizes the number of peaks, the possible vehicle types, and the estimate of the length that could be used. It should be noted that since the vehicle length estimate in this case is only used for developing the initial condition of the

18

loop characteristic function, it is not as critical as other applications, i.e., some estimation errors are permissible.

Table 3-1: Vehicle-length estimates based on peaks of waveform

No. of Peaks in the signature	Possible Vehicle Type	Length (in feet)
1	Passenger car/ van	21
2	Pickup truck	23
3	Delivery truck/ van	30
4	Truck	40
5	Semi trailer truck	58
>=6	Long truck with trailers	66

Once the vehicle length is estimated from the inductance signatures, speed is estimated and it is used to calculate the time it would take the vehicle to pass through the 6 ft sensing zone. The higher the estimated speed, the smaller is the length of the loop model since the vehicle passes quickly over the loop. Although the length of the loop model depends on the speed of the vehicle, the overall shape of the loop system function remains the same. We propose to model the loop system function using the cumulative distribution function of a Gaussian function based on the observation that the convolved output is always smooth. The loop system function should be symmetrical, and one half of that is modeled using:

$$H(x) = \sum_{i=0}^{x} \frac{1}{\sigma\sqrt{2\pi}} e^{-(i-\mu)^2/2\sigma^2} \tag{24}$$

where, μ = mean of the Gaussian function

σ^2 = variance of the Gaussian function.

The mean and the variance of the Gaussian are manipulated to obtain the required length of the loop model and they do not have any statistical significance. Figure 3.2 shows an example of the estimated loop system function using the formulation described above for a truck with length 66 ft traveling at a speed of 40 miles/hr.

Loop Model In Time Domain
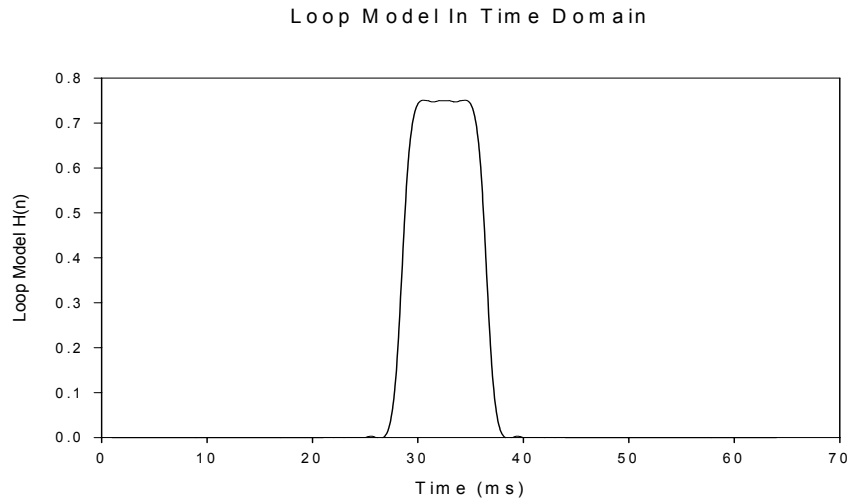
Figure 3.2: Estimated loop model of a semi-truck with 66ft of length traveling at 40 mph

4. PROCESSING STEPS FOR TRAVEL TIME COMPUTATION

4.1 Travel Time Processing Steps

The processing steps for travel time computation can be implemented as a sequence of modularized steps. Figure 4.1 shows the series of steps that are required to process the raw inductance data.

```
[End-Point Detection] → [Low-pass filter] → [Blind Deconvolution] → [Endpoint Detection]
                                                                           ↓
[Travel-Time Estimation] ← [Vehicle Re-identification] ← [Feature Extraction] ← [Normalization]
```
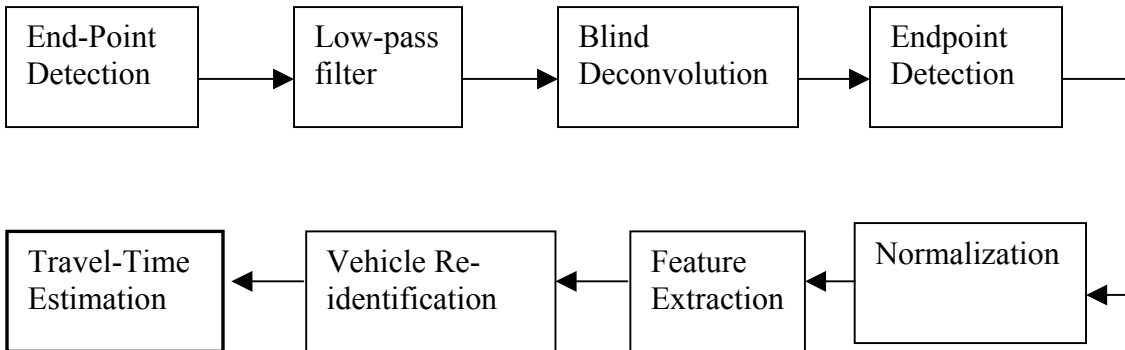
Figure 4.1: Travel time computational steps

Each of the steps is described in detail along with the method of implementation, the related problems, and their solutions.

4.2 Endpoint Detection

Since the raw data received from an ILD card is a continuous stream of sampled inductance data stream that includes idle states, the very first step before any analysis is to identify the beginning and ending of the vehicle presence in the waveform. This process removes the idle state and segments out only the vehicle signatures for the next processing steps. This process is referred to as the endpoint detection.

A number of methods can be used for endpoint detection. A simplest method is to check for zero crossing. However, this approach frequently fails due to the presence of noise. Another method would be to check when the channel signal crosses a certain threshold, but this approach again has its own problems due to shifts of idle levels. A proper threshold level depends on the noise characteristics and the surrounding environment. As a result, it does not stay constant. If the selected threshold is too low,

then there can be false threshold crossings due to noise. If the threshold is too high, then the start of the vehicle signature may be located well before the point where the channel signal crosses the threshold.

In this research, we decided to utilize the slope of the channel signal along with a rough cut by a relatively high threshold. The algorithm works as follows. First, the threshold method is used to crudely determine the start and end of the signature by setting the threshold level well above the channel idle noise level. This ensures not detecting noise as a vehicle. Second, using the slope of the waveform the starting and ending points are back tracked until the absolute value of the slope is reduced by a certain percent (typically 40% or more). Experimental results showed that this approach works best among the approaches that were tried in this study.

4.3 Low Pass Filtering and Blind Deconvolution

The next step is to implement the deconvolution techniques described in Section 3. To make this task simple it is desirable that all the signals are first converted to the frequency domain (i.e., using Discrete Fourier Transform). First, the complete channel signal is divided into segments of size N each (where N can be chosen from 256, 512, or 1024) and then each segment is converted to the frequency domain using N-point FFT. However, this method leads to a problem of ringing in the signal due to the Gibbs phenomenon when the vehicle signature is partly in one segment and partly in another. To rectify this problem, individual signatures were segmented out using the endpoint detection data and shifted so that the entire signature lies inside the N-point segment. This approach must be applied carefully. Segmenting out the individual vehicle waveform leads to an increase in the high frequency components in the frequency domain, which in turn introduces another undesirable ringing effect during the inverse filtering process. This problem is easily solved by a low-pass filter, which removes the sharp edge of the segmented waveform. A linear-phase low-pass filter with cutoff frequency of 0.5 with order 32 was designed and used for this purpose in this study. This step is shown in the second module in Figure 4.1.

Next, the individual waveforms are deconvolved using the techniques described in Section 3, i.e., Eqs. (15), (21), and (22). After obtaining the deconvolved signatures,

22

endpoint detection must be carried out once again. Recall that the convolution process by ILD is similar to smoothing by a moving average filter. Hence, reversing the smoothing by deconvolution introduces high-frequency components in addition to the restored signal and causes changes in the end points. This is the reason that another end-point detection is needed after deconvolution.

4.4 Normalization

After deconvolution and end-point detection, a few basic signal issues need to be addressed. The first issue is that the amplitude, the height of signatures, of the same vehicle varies from one loop to another. This is predictable since the vehicle may not pass the loops the same way, and some differences may always exist between any two loop installations. Hence, some kind of amplitude normalization is required. However, we cannot scale all of the signatures to the same amplitude since it would destroy the information about the height of the vehicles. To achieve both, i.e. to keep intact the height information of individual signatures and still have a common ground for comparing the vehicle signatures of the same vehicle for different locations, a channel amplitude normalization approach was used as follows. The maximum for each deconvolved channel signal is calculated, and then each signature is divided by the channel maximum from which a channel-wise normalization is achieved.

Another issue that needs to be addressed is that the length of signature is partially a function of vehicle speed, i.e., faster speeds create shorter signatures. The length of the signature also depends on the length of the car. Hence the signature of a small car driven at a slow speed may have the same length as that of a longer car driven at a higher speed. This ambiguity was resolved by using a re-sampling and filtering technique. This issue of signature length normalization is discussed further in section 5.4.

4.5 Feature Extraction

The signatures obtained after deconvolution disclose more details as compared to the unprocessed waveforms. These details, such as number of peaks and valleys, and their relative positions and heights, give the signature a characteristic shape. The feature

23

extraction employed in this study is to find the number of peaks and valleys for all of the signatures, since they are the defining features of the signature.

4.6 Vehicle Re-identification by Pattern Matching

To find the matching signature more efficiently, first the likely matching signatures can be identified or designated. This can be done by calculating a probable window of the time during which the vehicle will reach the downstream detector. This window can be estimated using the speed estimate at the upstream detector and the distance between the two detectors. All the signatures in this window are then considered the likely candidates.

Various methods were tried out for matching the signatures in this research. The first approach tried was the cross-correlation coefficient approach. In this case, the point where the cross-correlation coefficient achieves the maximum is the point of matching. Although cross-correlation is a commonly used pattern matching technique, it did not yield satisfactory results. Another approach worked better, and is described below.

Denote the N possible candidates of the segmented matching signatures as $Y_i(t)$, $i=1,...,N$. The signal of the candidate signature i extends from t_i to $t_i + l(Y_i) - 1$ where $l(Y_i)$ is the length of the signature. Let the reference signature be denoted $X(t)$ and the signal extends from 0 to $l(X) - 1$ where $l(X)$ is the length of the signal supporting area. In this approach, $X(t)$ is moved over $Y_i(t)$ and the difference coefficient is calculated using the following equation for every point s,

$$\gamma_i(t_i + s) = \frac{\sum_{t=t_i}^{t_i+s} |[Y_i(t) - \overline{Y}_i] - [X(t + l(X) - s - t_i) - \overline{X}]|}{s+1} \tag{25}$$

where s goes from 0 to $l(Y_i)$, $\overline{Y}_i$ denotes the mean of $Y_i(t)$ and $\overline{X}$ denotes the mean of $X(t)$. The position $t_i + s$ at which $\gamma_i(t_i + s)$ is minimum is considered the matching point for that probable match and is used later to estimate the travel time.

For every probable candidate signature, the overall difference coefficient is calculated as the summation of three parameters, i.e., minimum difference coefficient given by Eq. (25), difference of the number of valleys, and difference of the number of

peaks of the inductance signatures. In summary, the overall matching score for a signature i with any of the probable match j is computed by:

$$\Delta_j = |\min_s[\gamma_j(t_j + s)]| + |Peaks(i) - Peaks(j)| + |Valleys(i) - Valleys(j)| \quad (26)$$

The matching signature is the one for which this matching score is minimum and the vehicle is claimed as the re-identified vehicle.

4.7 Travel Time Estimation for Individual Vehicles

After the two signatures have been identified as matching signatures (signatures of the same vehicle), the next step is to decide the point in time where the maximum similarity shows. This step is necessary to decide which time stamp for each channel should be considered for calculating the travel time. A few methods for this purpose are listed below.

1. Time interval between points where the signatures cross the 10% threshold
2. Time interval between points where the signatures drop below the 10% threshold
3. Time interval between 50% point of both the signatures
4. Time interval between the maximum peaks of both the signatures
5. Time interval between the points where difference coefficient is minimum

According to the tests this study conducted, it was found that method–5 gave the best results since the difference coefficient computed using Eq. (25) is minimum at the point where the signatures show the maximum similarity. This method works as follows. First, the signature to be matched is moved to the left of its support area, and then gradually shifted to the right until they do not overlap. In that shifting process, the position S_1 where the difference coefficient (given by Eq 25) is minimum is determined, i.e., S_1 is the position in which the autocorrelation is maximum. Next, the matching signature is moved to the signature identified from the downstream station and then shifted the same way. The position S_2 where the difference coefficient is a minimum is then determined. Finally, the difference between the time stamps at the positions S_1 and S_2 is recorded as the estimated travel time.

4.8 Treatment of Travel-Time Estimation from Unidentified Vehicles

The accuracy of individual vehicle re-identification rate is not likely to reach 100% since some failures and exceptions are always expected. It is also likely that the failures of re-identification will be scattered among the identified vehicles. It should be noted that in the proposed system the arrival time of each vehicle is known whether the vehicle was identified match or not. Hence, if a set of vehicles, formed by unidentified and identified, is carefully analyzed along with their arrival times, it is possible to derive a method that the final average of the travel time is improved. This could be analyzed using the following assumption. Suppose that the algorithm was not able to identify most vehicles except few. Therefore, only the arrival times of unidentified vehicles were recorded at the upstream and downstream of a highway section. A group of vehicles are selected according to uniform distribution of arrival times near the identified vehicles. This means that the selected vehicles were maintaining similar distances. Under this assumption, we wish to identify the average travel time of this vehicle group. This travel time is referred to as the group travel time.

Consider that the timestamps recorded at the upstream station are F_i (for $i = 1$ to n) and the timestamps at the downstream station are S_i (for $i = 1$ to m), where n is the number of vehicles in the group at the upstream station and m is the number of vehicles in the group at the downstream station. Notice that m and n may not be equal since we cannot guarantee that the headway distribution will retain their structure as they pass from one station to another, i.e., some vehicles may exit from the measuring segment of the highway. Since our objective is to find the statistical average of travel time, small variance caused by such cases should not affect the final outcome. Below, four computational methods of group travel time are discussed.

1. The vehicle at the ith position at the upstream station can be at any j^{th} ($j = 0$ to m) position when the group reaches the downstream station. The travel time T_i for the ith vehicle at the upstream station can then be estimated using

$$T_i = \frac{\sum_{j=1}^{m}(S_j - F_i)}{m} \qquad (27)$$

Hence, the average travel time taken for the entire group to travel from the upstream station to the downstream station is given by

$$GroupTravelTime = \frac{\sum_{i=1}^{n} T_i}{n} \qquad (28)$$

2. A group of vehicles may be treated as a single entity. The group travel time then can be estimated as the difference between the average of arrival times at the upstream station and the average of arrival times at the downstream station, i.e.,

$$GroupTravelTime = \frac{1}{m}\sum_{j=1}^{m} S_j - \frac{1}{n}\sum_{i=1}^{n} F_i \qquad (29)$$

3. Instead of finding the average of all arrival times, only the average of the head and tail of the group is considered for the computation, i.e.,

$$GroupTravelTime = \frac{(S_1 + S_m)}{2} - \frac{(F_1 + F_n)}{2} \qquad (30)$$

4. The methods 1-3 do not take into account the outliers. Hence, a more robust method is to compute the group travel time after removing the outliers from the group. Various tests and algorithms can be used to detect the outliers. One simple way to detect outliers is to compare the absolute difference between the sample and the group median to a preset threshold. After removing the outliers, the second method is used to compute the group travel time.

$$GroupTravelTime = \frac{1}{m'}\sum_{j=1}^{m} r(S_j) - \frac{1}{n'}\sum_{i=1}^{n} r(F_i) \qquad (31)$$

where $r()$ is a robust function that removes the outliers, and m' and n' are the count after removing the outliers.

Among the above methods, method 3 is considered least reliable since it is prone to be influenced by outliers. It is also reasonable to covert Eq. (28) or (29) to a weighted average. Method 4 is a special case of weighted average where outliers are given zero weights and the rest are given unit weights. Method 4 would be most reliable among the approaches discussed.

5. EXPERIMENTAL RESULTS

5.1 Data Collection

5.1.1 Highway data

For this study, the ILD waveform data was collected from the 3M-research site located near the I-35W/I-494 intersection in Richfield, Minnesota. This site contains many different types of loop installations for testing the effectiveness of loop configuration. The data was collected in pairs of loop detectors, one from an upstream location and the other from a downstream location, 60 ft apart. Since both loops are terminated at the same control cabinet, we were able to collect data in a single file with synchronized time. The types of loop cards used are Canoga C800 series. The change in inductance was recorded approximately every 10 milliseconds along with a time stamp. The loop detector cabinet and laptop PC setup used for data collection are shown in Figure 5.1. Data was captured by connecting the laptop computers to the communication port of the Canoga card. For verification of vehicle identification, a high-speed video recording system was used to record the vehicles passing over the detector along with a time stamp (Figure 5.2). The 3M Company specifically designed this video system to synchronize with loop detector actuation, and millisecond time stamps were embedded in the video image. For our experiments, this video recording was used for visual verification of re-identification.
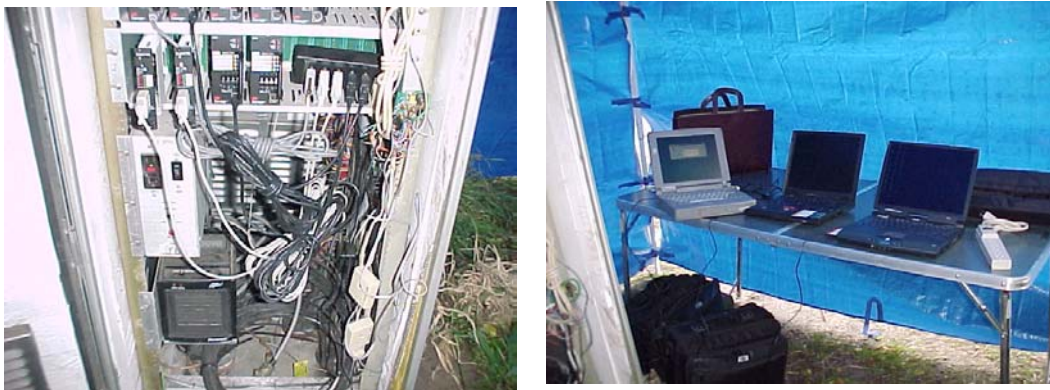
Figure 5.1: Data collection equipment: left=detector cabinet, right=laptop computers

Figure 5.2: Video recording system with loop actuation and timestamp

5.1.2 Data collection for impulse response of loop system

      An attempt was also made to collect data to estimate the impulse response of the loop system. For this purpose, a steel pipe fitted with two wheels at both ends was moved over a loop and the change in inductance was recorded (Figure 5.3). The idea was that as the pipe cuts through the magnetic flux of the loop, there would be a change in inductance, which will be very close to the impulse response of the ILD system. However due to the limited metal surface of the pipe and the low sensitivity of the inductance loop, the data failed to show any changes in inductance when the pipe was moved over the loop. This experiment did not yield the impulse response of the system function.

Figure 5.3: Apparatus used for loop system impulse response

A better approach for creating an impulse input could have been to use a vertical sheet of steel to create a large surface to form a sufficient amount of eddy currents. This attempt was not made due to the difficulty of building such an object and effectively moving the object over the loop. It was also uncertain whether movement of a large sheet would work as an impulse input or not. It was concluded that finding the impulse response of an ILD system using a physical input is difficult since it must be a 3-dimensional physical input. Thus, the research team decided to leave the ILD system as a blind system.

5.1.3 Waveforms on different speeds of the same vehicle

In order to check the ability of the algorithm to match signatures collected at different speed, a set of inductive waveforms of the same car at different speeds was collected. For this purpose, inductive waveforms for a Ford Ranger (Axle Length =10' 5.7" and Height=1' 9") were collected at four different speeds (10mph, 20mph, 30mph, 39mph). The vehicle used is shown crossing the loop in Figure 5.4.

Figure 5.4: Ford Ranger used to collect inductance waveforms at various speeds

5.2 CLS Deconvolution Examples

5.2.1 Effect of deconvolution

The effect of CLS deconvolution is demonstrated using inductance waveforms of two passenger vehicles. The data used for this portion was collected from the 3M loop research site. The data is organized as two channels in which the first channel is the data stream recorded from the upstream station and the second channel is the data stream recorded from the downstream station. The waveforms of the two vehicles used in this example are shown in Figure 5.5. In the graph, the data from the upstream station was depicted as a solid line (Ch0) and the data from the downstream station was depicted as a dotted line (Ch1). Thus, the first pair of solid and dotted waveforms is the first vehicle and the second pair solid and dotted waveforms are the second vehicle. It can be clearly observed in the graph that the waveforms are extremely smooth indicating the effect of loop convolution. From this graph, we can deduce that the ILD system function is a smoothing function such as the function described in Section 3.4.
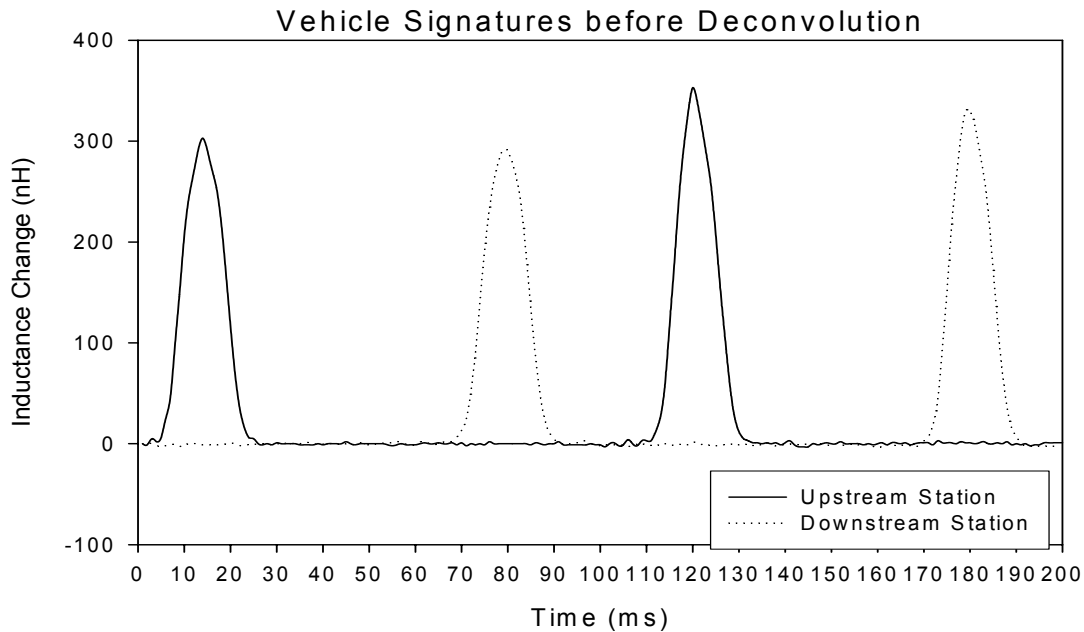
Figure 5.5: Inductance waveforms of two passenger vehicles recorded at two separate stations

31

We now show the effect of CLS deconvolution. The inductance waveforms in Figure 5.5 were processed using Eq. (15) with *H* designed as a simple rounded square wave in time domain. For computation, 256 FFT and Inverse FFT (IFFT) were used. The result is shown in Figure 5.6. Notice in the waveforms that the details are recovered from the smoothed signal showing the differences in the basic shape. Before the deconvolution, all of the four signatures had very similar shape characteristics, so it was very difficult to discriminate between them. Figure 5.6 now clearly shows the differences between the two vehicles which can be used as vehicle features. The first vehicle can be characterized as two peaks with equal height, and the second pair can be characterized by a higher first peak and a shorter second peak. It can be also noticed that the vehicles had two axles, characterized by the two peaks. These distinguishable characteristics lead to a higher rate of vehicle re-identification. However, the deconvolution process also adds noise to the signature, so proper filtering is required after the deconvolution.
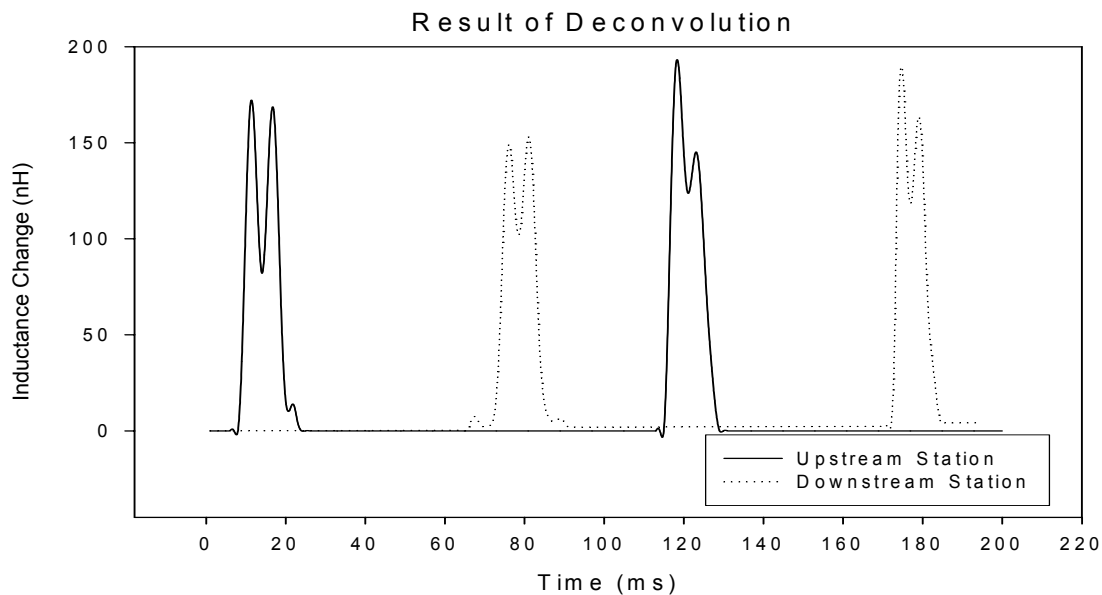
Figure 5.6: Results of deconvolution

5.2.2 Comparison example of three vehicles of similar length

The raw inductance waveforms show only minute differences as long as the vehicle length is similar. Figure 5.7 shows three vehicles of completely different types and their waveforms along with the video images. In the graph, the solid lines show the raw inductance waveforms before deconvolution, and the dotted lines show the signature obtained after the deconvolution. Notice that all three solid line signatures have a similar shape and do not expose clearly distinguishable features even though the vehicles are completely different. Now notice the signatures obtained after the deconvolution (shown by the dotted lines). They clearly show distinguishable features that can be characterized by the peak and valley types.

Passenger car   Van   Pickup truck
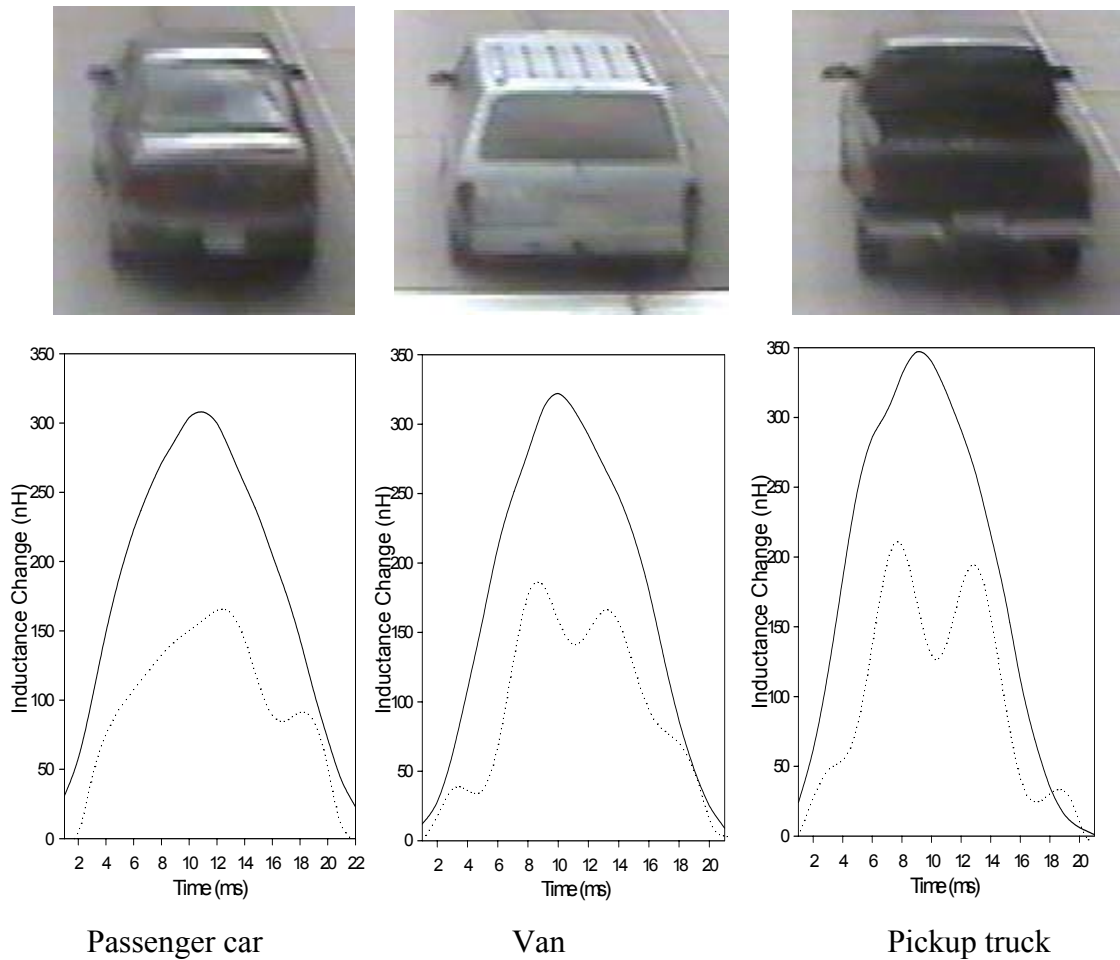
Figure 5.7: Comparison of vehicles with a similar length: before CLS deconvolution=solid line, after deconvolution=dotted line

5.2.3 Comparison example of three vehicles with the same type

In order to answer the question on how the deconvolution would perform if the vehicles are in the same class, we selected three passenger cars. Figure 5.8 shows three different passenger cars and their waveforms. The top-row images are the corresponding vehicles. These vehicles were traveling approximately 68 mph. It can be clearly seen that all three solid-line signatures have a similar shape and characteristics, and fail to provide any discriminating information about the vehicle. On the other hand, the waveforms obtained after deconvolution clearly show different shapes for all three vehicles. More specifically, the number of peaks and valleys, and the sizes are clearly distinguishable.
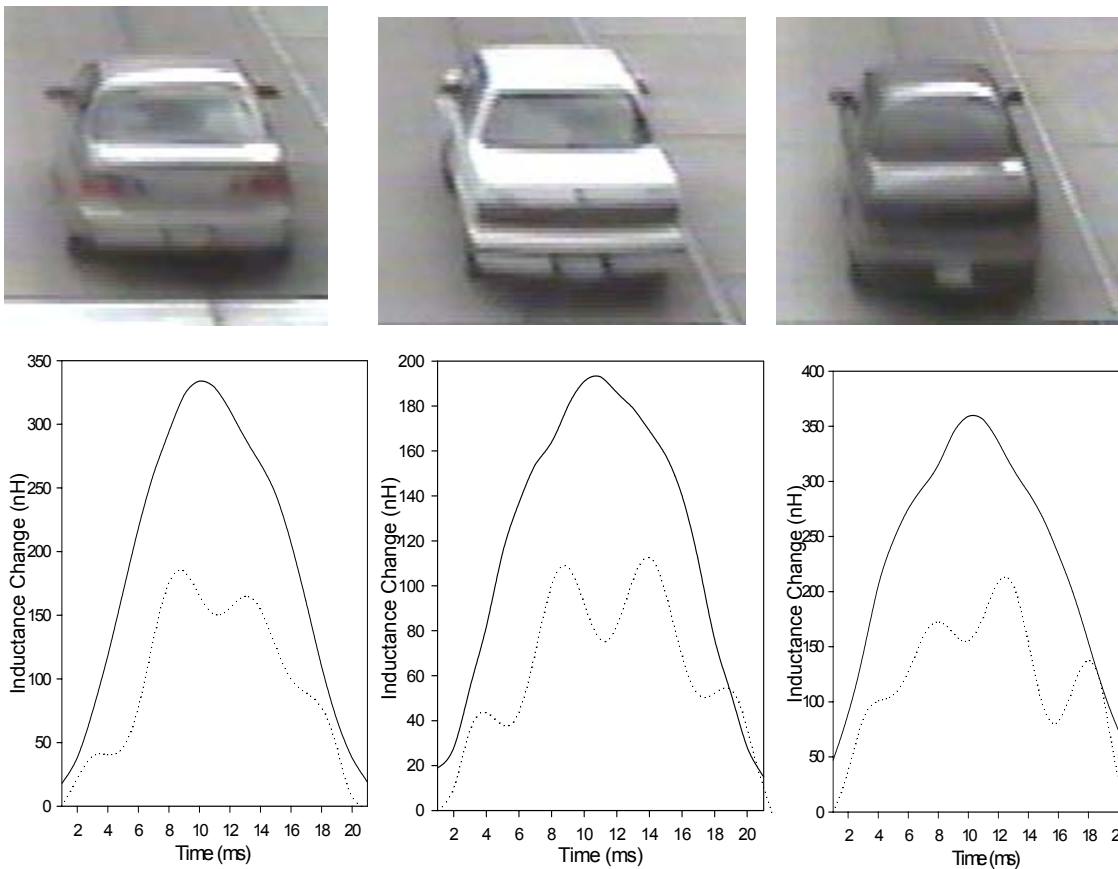
Figure 5.8: Comparison of three passenger cars: before CLS deconvolution=solid line, after deconvolution=dotted line

5.2.4 Re-identification Example-1

This example illustrates re-identification based on the deconvolved waveforms. Figure 5.9 shows vehicle signatures before (solid line) and after deconvolution (dotted line). The upstream signature shown in (a) is compared with three downstream signatures (b)-(d). The matching scores were found to be (b)=10, (c)=25, (d)=17, so the minimum is the downstream signature (b). Hence, the upstream signature (a) is matched to downstream signature (b). This is indeed a correct match verified by the vehicle images.
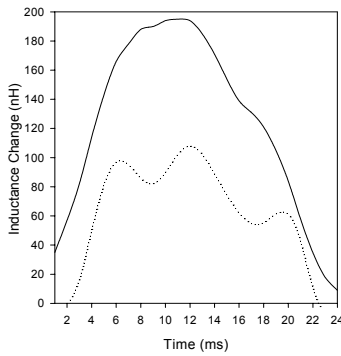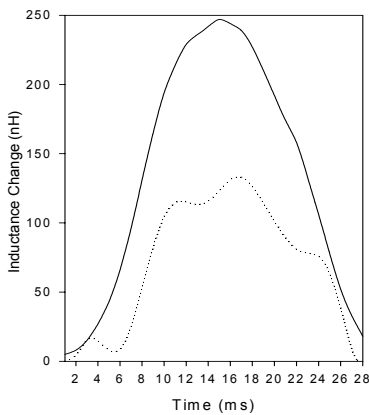
(a) Upstream
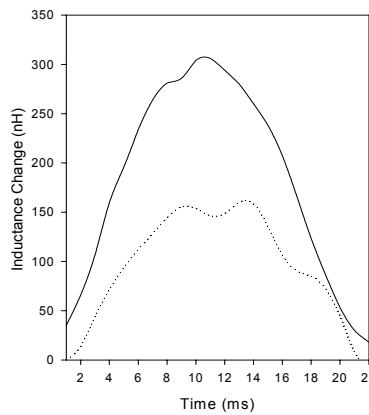
(b) Matching Score=10   (c) Matching Score =25   (d) Matching Score =17
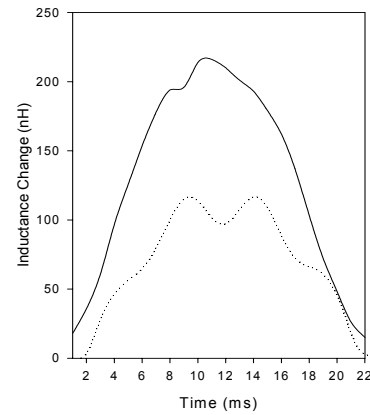
Figure 5.9: Vehicle re-identification. (a) is the upstream vehicle, and (b)-(d) are possible match candidates of the downstream vehicles. (Before deconvolution=solid, after deconvolution=dotted).

35

5.2.5 Re-identification Example-2

This example illustrates a failed case of re-identification. The waveforms before and after deconvolution are illustrated in Figure 5.10. The upstream signature is compared with three downstream signatures (b)-(d). The matching scores were (b)=14, (c)=12, (d)=22, so the upstream signature (a) was matched to the downstream signature (c). However, the correct match in this case is (b). In this case, the re-identification algorithm was not successful in finding the correct match. However, we can visually verify that (b) is a better match according to the shape of the main peaks.

(a) Upstream

(b) Matching Score=14   (c) Matching Score =12   (d) Matching Score =22
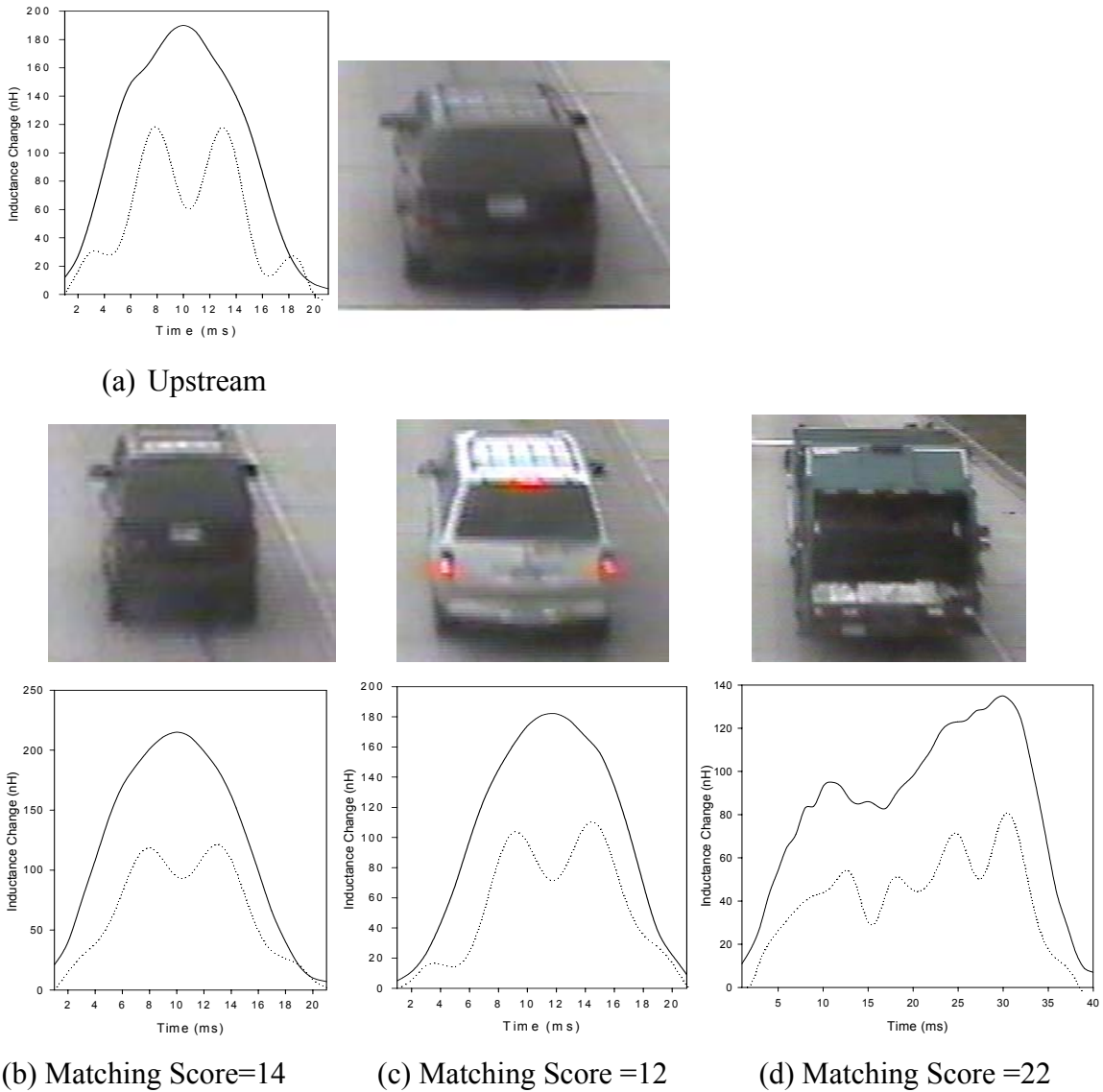
Figure 5.10: An example of vehicle re-identification failure. (a) is the upstream vehicle, and (b)-(d) are possible match candidates at the downstream vehicles.

5.3 Godard Blind Deconvolution Examples

This sub-section repeats the earlier examples using the Godard blind deconvolution. In all examples, the vehicle signatures before the Godard blind deconvolution are shown by solid lines and the signatures obtained after the Godard deconvolution by dotted lines.

5.3.1 Comparison example of three vehicles of similar length

Figure 5.11 shows three vehicles of different types and their signatures. It can be seen that all three waveforms before the deconvolution have similar shape characteristics and fail to provide detailed information about the vehicle. However, the waveforms obtained after the Godard blind deconvolution show features that are more distinctive.
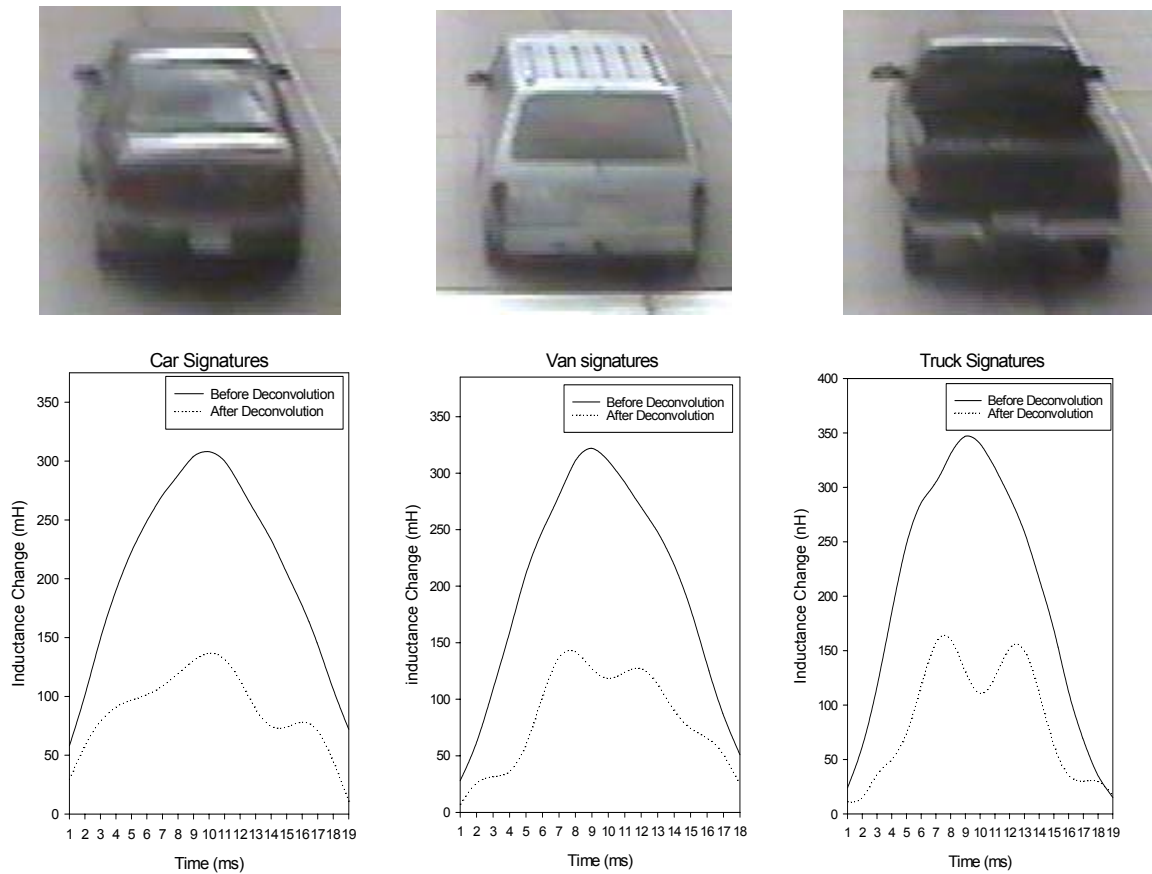
Figure 5.11: Comparison of vehicle waveforms with a similar length before and after Godard blind deconvolution. The three vehicles are a car, a van, and a pick-up truck.

5.3.2 Comparison example of three passenger car vehicles

Figure 5.12 shows three different passenger cars and their signatures after the Godard blind deconvolution. Since all of them are the same type, the signatures before the Godard blind deconvolution are very similar. However, the signatures obtained after the Godard blind deconvolution clearly show distinguishable shapes for all three vehicles. Since the characteristics of each individual vehicle's signature can be more uniquely defined, this will help increase the re-identification rates.
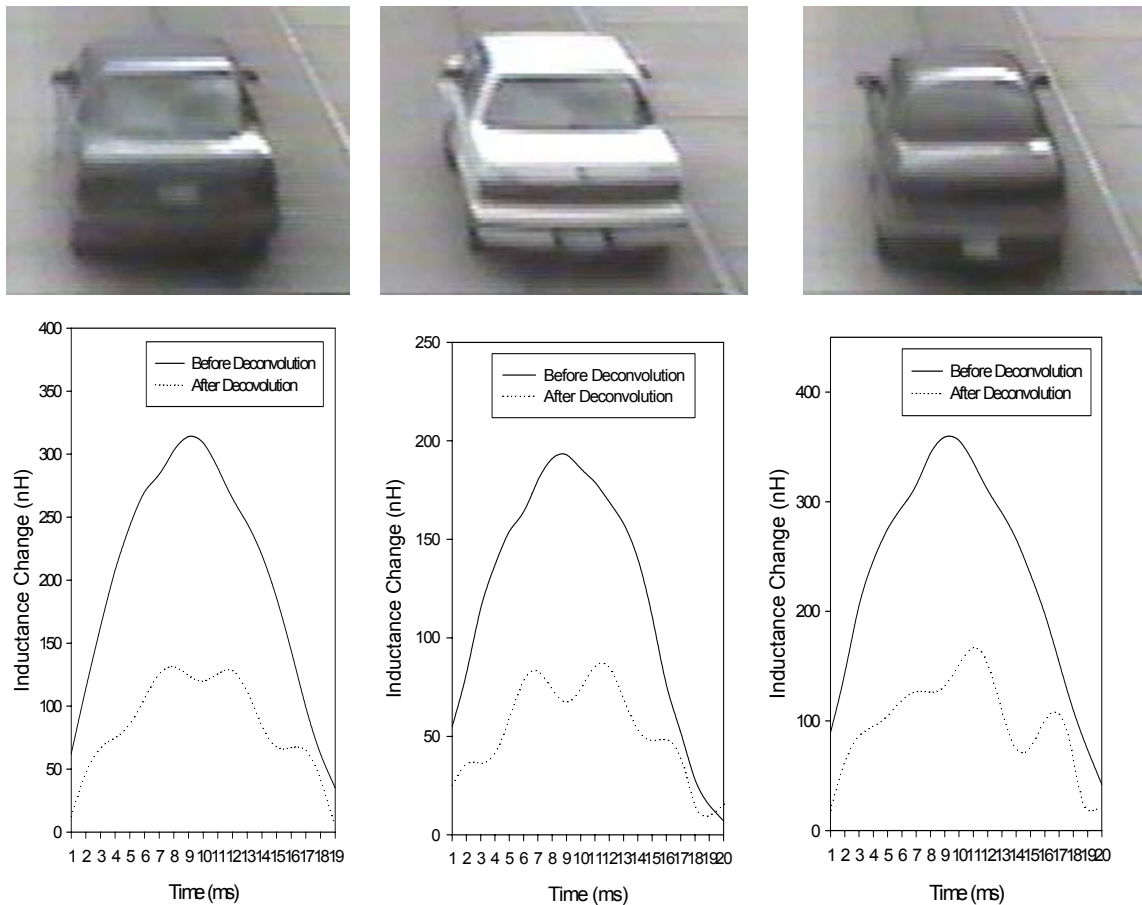
Figure 5.12: Comparison of three passenger cars before and after deconvolution: before=solid line, after=dotted line.

5.3.3 Re-identification Example-1

This example illustrates re-identification based on signatures after the Godard deconvolution (Figure 5.13). The upstream signature shown in (a) is compared with the three downstream signatures (b)-(d). The matching scores were found to be (b) 12, (c) 27, (d) 29, so the minimum in this case is the downstream signature (b). Hence, the upstream signature (a) was correctly matched with the downstream signature (b) by the algorithm, as verified by the vehicle images.

(a) Upstream

(b) Matching Score=12   (c) Matching Score =27   (d) Matching Score =29
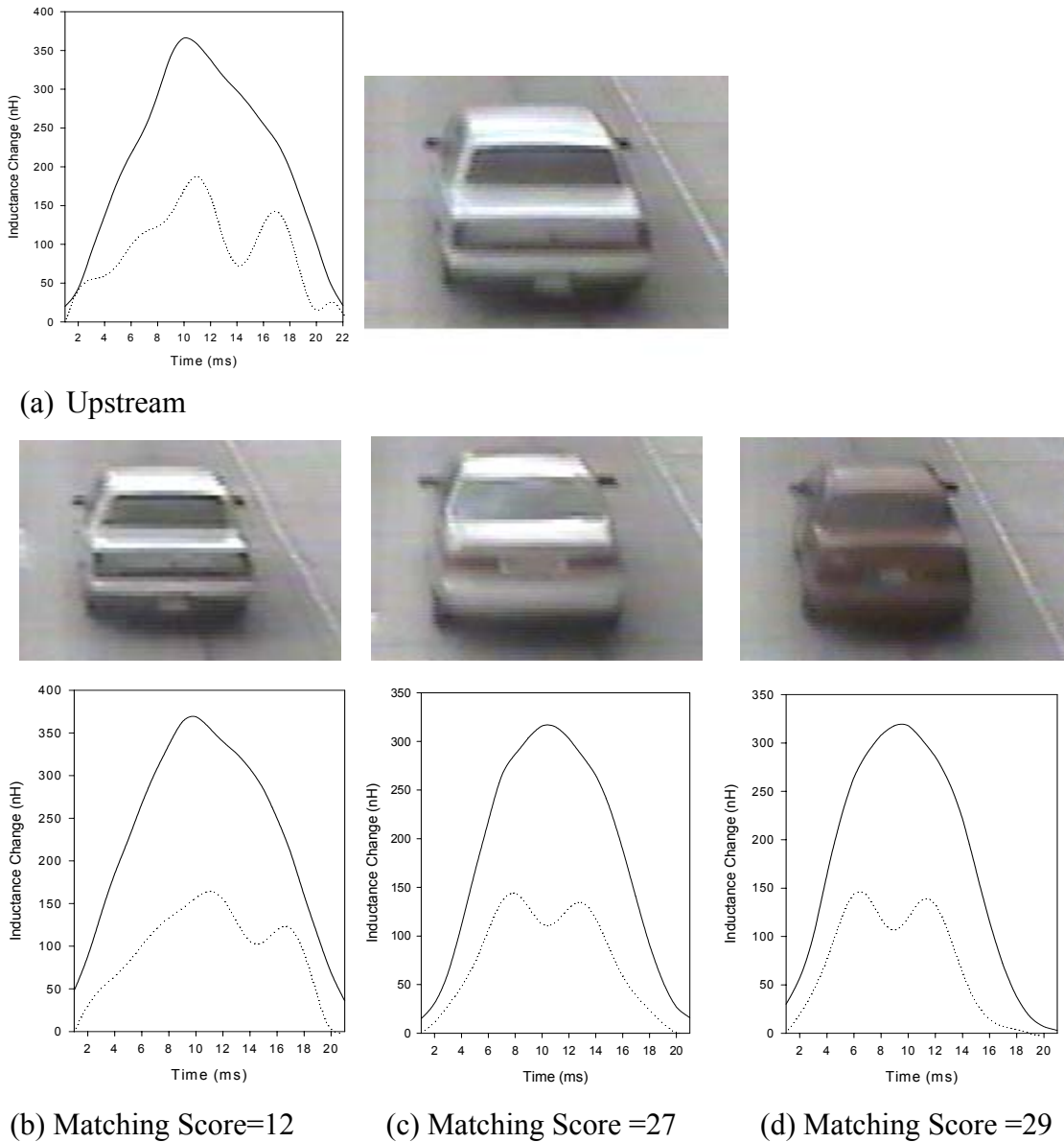
Figure 5.13: Vehicle re-identification example. (a) is the upstream vehicle, and (b)-(d) are possible match candidates of the downstream vehicles.

5.3.4 Re-identification Example-2

This example illustrates the failed case of re-identification by the pattern matching algorithm (Figure 5.14). The matching scores were found to be (b)=12, (c)=17 and (d)=11, so the algorithm determines (d) as the best match, which is not correct. In this case, the pattern matching algorithm simply made a mistake. The curve shape of (b) is clearly a better match according to visual inspection. However, it is interesting to notice that the algorithm finds (c) as a much more different vehicle as compared to (b) and (d), which is true according to the images of the vehicles.

(a) Upstream

(b) Matching Score=12   (c) Matching Score =17   (d) Matching Score =11
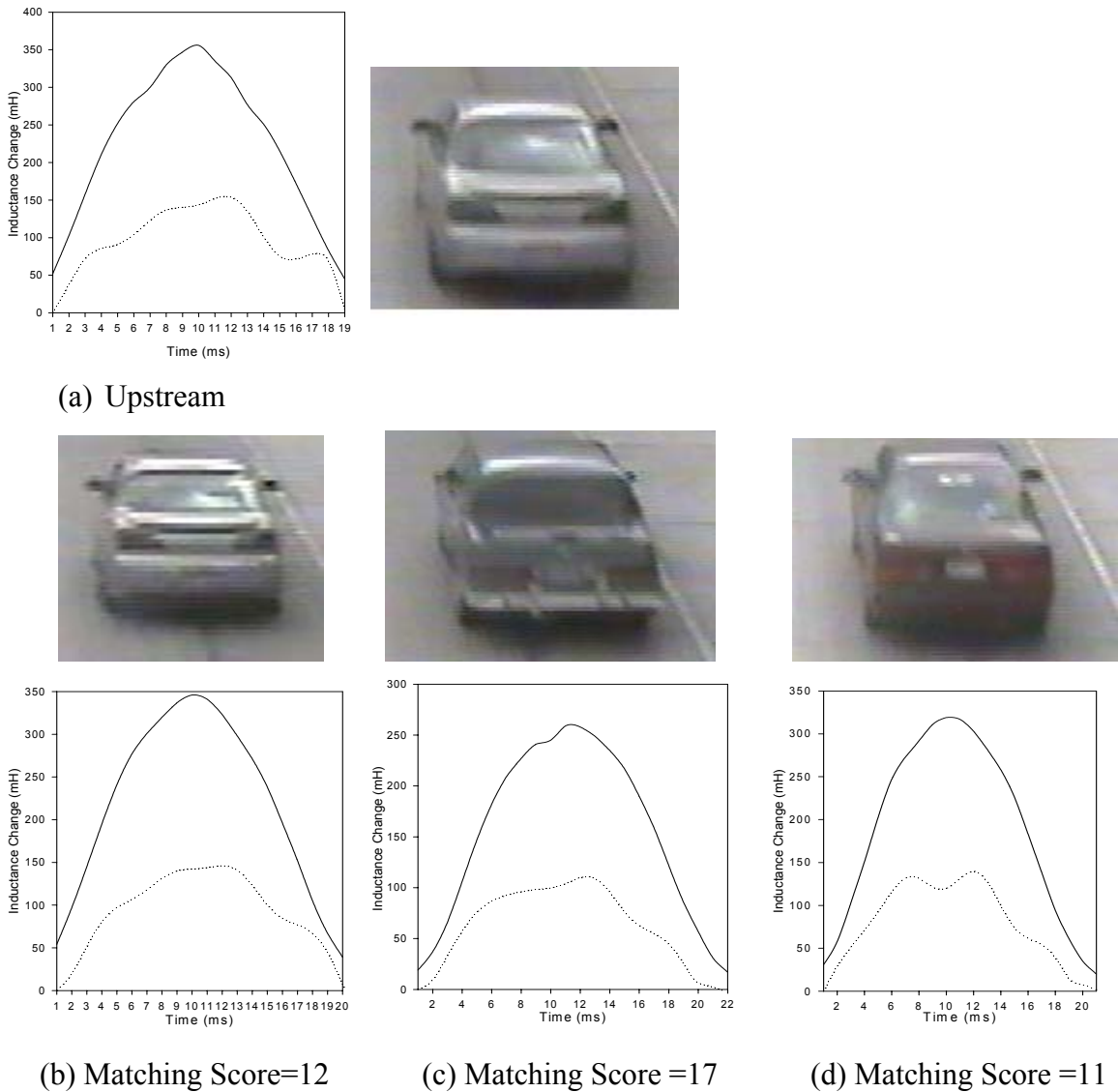
Figure 5.14: A failed case of vehicle re-identification. (a) is the upstream vehicle, and (b)-(d) are possible match candidates of the downstream vehicles.

5.4 Speed Normalization

As mentioned in Section 3, the length of the inductance waveforms not only depends on the length of the vehicle but also on the speed of the vehicle. The effect of speed and the related normalization techniques are discussed. In Figures 5.15 and 22, the dotted line represents the raw inductance signatures for the same vehicle driven at 10 mph and 39 mph respectively. This data was taken using a Ford Ranger as described in Section 5.1.3. Notice that the length of the signature in Figure 5.15 (10 mph) is nearly four times that of the one in Figure 5.16 (39 mph), since the speed ratio is four to one. This means that some kind of speed normalization will be required to make the signature characteristic be irrespective of the speed.
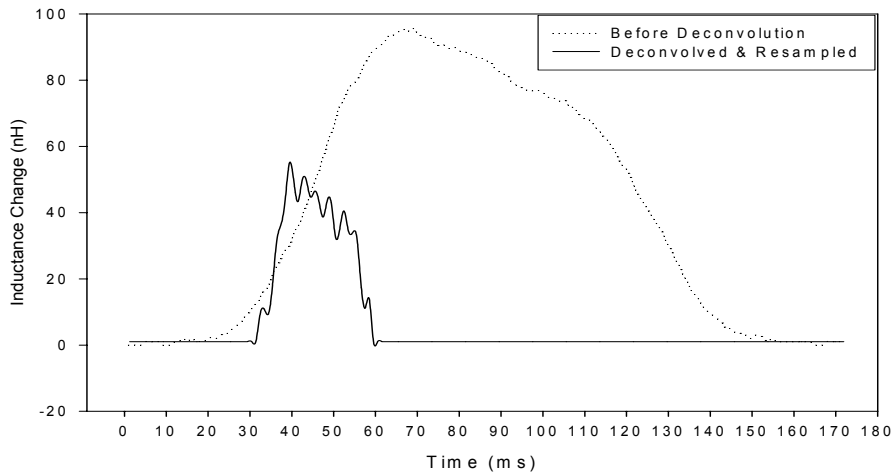
Figure 5.15: Original (dotted) and deconvolved and then re-sampled (solid) signature of Ford Ranger driven at 10mph
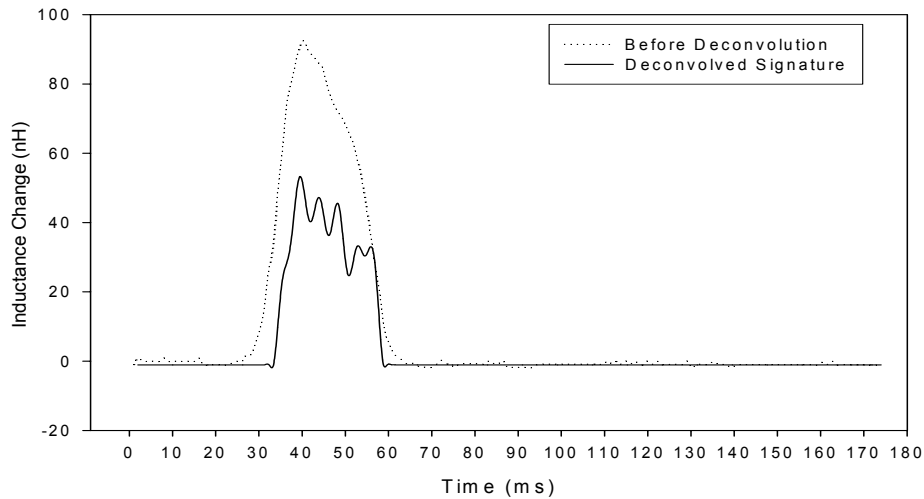
Figure 5.16: Original (dotted) and deconvolved (solid) signature of Ford Ranger driven at 39mph.

A simple but effective approach is to normalize the vehicle signature to a length equal to the length of the shortest signature (fastest speed). The idea behind this approach is that, since the shortest signature contains the least information, the other comparing signatures are time normalized to the shortest. To this end, we first compute the sample ratio k by,

$$k = \frac{\text{No of samples of comparing signature}}{\text{No of samples in the shortest signature}} \tag{32}$$

The first method devised to convert to a normalized waveform was to compute the new samples by averaging k samples. In all, M new samples are computed where M is the number of samples in the shortest signature. Hence, the new signature obtained has the same length as the shortest signature, providing the same length for different speeds.

The second method devised was to resample the longer signatures to the shortest length. As shown in the block diagram in Figure 5.17, the deconvolved signature is first passed through a low pass filter in order to remove high-frequency components. This low pass filter is designed with a cutoff frequency of ω given by,

$$\omega = \frac{(0.5\pi)}{k} \tag{33}$$

The filtered signature is then down-sampled by taking every k^{th} sample. However, if k is a fraction then linear interpolation is used to find the value of the sample at $n*k$ (where $n=1,2,...M$).

Experimental results show that the re-sampling of a low speed signature retained more precise pattern characteristics of the higher speed signature. In Figure 5.15, the solid line waveform is the re-sampled signature obtained when the speed of 10 mph was normalized to 39 mph. The solid line waveform in Figure 5.16 is the deconvolved signature at the speed of 39 mph. Both signatures show similar peak patterns with little differences in the relative height of the peaks. The re-sampled signature also shows two irregularities at the beginning of the leading edge and at the end of the trailing edge. These can be attributed to the non-uniform speed while passing over the loop since it is extremely difficult to keep the speed constant at 10 mph. However it is much simpler to

keep the speed uniform at a higher speed, hence these irregularities are absent in the 39 mph signature. As demonstrated by this example, speed normalization can be used to obtain the patterns of deconvolved signatures that are independent of the vehicle speed.
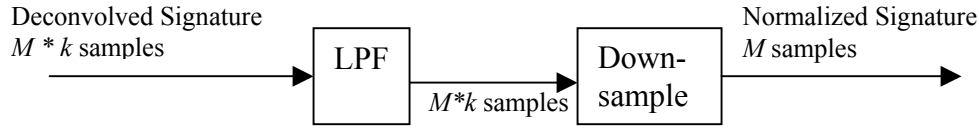
Figure 5.17: Speed normalization down-sampling

5.5 Overall Performance of Re-identification

During the data collection process, two large data sets named "Test1.dat" and "Test2.dat" were collected from the 3M loop test site. The test site on the freeway had three lanes, but the inductance signatures were collected only from one of the lanes. The shapes of loops were different from the upstream to the downstream stations. Test1.dat was collected from vehicles traveling over a circular loop (upstream) and a square loop (downstream). Test2.dat was collected from the middle lane which had a diamond loop at the upstream and a square loop at the downstream. Therefore, the loops were not uniform, which should introduce more challenges for the detection algorithm.

The two deconvolution approaches, i.e., CLS filter and Godard deconvolution were tested for re-identification rates, and Table 5.1 summarizes the overall performance of the two approaches. The re-identification rate was computed using the following:

$$Reidentification\_Rate = \frac{\text{Num of upstream vehicles found at downstream}}{\text{Num of upstream vehicles}} \times 100$$

In addition to the re-identification rates, the table includes computer execution time of various computation steps and the number of vehicle signatures in the data set.

According to the test results, the re-identification rate of signatures after the Godard blind deconvolution was slightly higher than that of the CLS deconvolution for the Test1.dat data. On the other hand, the CLS deconvolution showed a slightly better performance with Test2.dat. The re-identification rates of both methods should be considered similar since the difference was small and dependent on the data. Of the 563

43

vehicles in Test1.dat, the pattern-matching algorithm after Godard Blind Deconvolution failed to re-identify only 56 vehicles at the downstream station. The average re-identification rate of all four tests (Table 5.1) was about 89%, which is considered very high in comparison with the past research reports. However, this performance is not directly comparable since the data sets used are different. Another important performance factor is the computational time. It was found that the Godard deconvolution approach required a much longer computational time due to its repeated iteration steps as compared to a single step in the CLS deconvolution. Godard deconvolution still has the advantage that the knowledge about the precise loop-system function is not required.

Table 5-1: Performance results of the 3M test data

Method	CLS Deconvolution		Godard Blind Deconvolution	
File Name	Test1.dat	Test2.dat	Test1.dat	Test2.dat
No. Of Signatures	563	760	563	760
File Size	1533 KB	4030 KB	1533 KB	4030 KB
Splitting time	1.315 sec	1.641 sec	1.188 sec	1.578 sec
Filtering Time	5.516 sec	7.172 sec	401.672 sec	660.375 sec
Feature Extraction Time	0.047 sec	0.047 sec	0.031 sec	0.031 sec
Matching Time	0.234 sec	0.313 sec	0.203 sec	0.344 sec
Re-identification Rate	**89.88%**	**88.82%**	**90.05%**	**85.92%**

The pattern-matching algorithm was also run for the raw vehicle waveforms (before deconvolution) to compare the identification rates with the deconvolved waveforms. Table 5.2 summarizes the re-identification rates obtained before and after deconvolution. In the table, "the difference coefficient threshold" indicates the ceiling value of the difference coefficient that the correct match should not exceed. If the difference coefficient of the matching signature was greater than this threshold, then the algorithm declared that sufficient similarities do not exist to claim re-identification. In essence, the threshold on the difference coefficient provides a means to eliminate those cases where re-identification is marginal.

In summary, higher re-identification rates were achieved for the data set Test1.dat after deconvolution when the threshold was set low, while no significant improvements

were observed for Test2.dat. Two observations could be made from these experiments. Test2.dat was at a free-flow state of traffic, and the data was collected from diamond loop to square loop. On the other hand, Test1.dat was collected from vehicles traveling from a circular loop to a square loop and under the traffic state with a higher travel-time variance or slightly congested. Therefore, the re-identification task for Test2.dat data was little bit easier than that of the Test1.dat data, and the blind deconvolution did not help improve the re-identification rate. The observation was that deconvolution improved the re-identification performance under the conditions with more irregular forms of loop shapes and higher variances in traffic flow.

These overall experiments suggest that the study should be extended to a larger set of data collected under a variety of traffic conditions in order to validate the benefits of blind deconvolution. In addition, the difference coefficient algorithm developed as the pattern matching algorithm for this study did not fully take advantage of uniqueness of the features exposed by deconvolution. In the future, a more sophisticated pattern-matching algorithm should be developed for the pattern identification.

Table 5-2: Re-identification rates for the 3M test data with threshold on the difference coefficient

Difference Coefficient Threshold	Without Deconvolution		CLS Deconvolution		Godard Blind Deconvolution	
	Test1.dat	Test2.dat	Test1.dat	Test2.dat	Test1.dat	Test2.dat
13	56.13%	89.87%	74.25%	88.42%	87.39%	85.39%
15	73.16%	89.87%	82.24%	88.62%	88.81%	85.79%
17	82.42%	89.87%	86.32%	88.82%	89.88%	85.79%
19	86.5%	89.87%	87.74%	88.82%	89.88%	85.92%

5.6 Real-Time Implementation Aspects

In real-time applications, the computational time is vital. The success of a real-time system depends on whether the computations can be done between the arrivals.

According to the computational time measured and shown in Table 5.1, the CLS deconvolution for 563 signatures took 5.43 seconds (10 milliseconds per signature) and the pattern matching took 0.29 seconds (0.5 milliseconds per signature) for the Test1.dat data. Therefore, the CLS deconvolution is applicable for real-time applications. For the same data, Godard deconvolution took 0.7 seconds per signature and the pattern matching

took 0.4 milliseconds per signature. Less than one second should satisfy the real-time requirements for a single-lane implementation. For multiple lanes, a dedicated digital signal processor system instead of a PC could be used to meet the real-time computational requirements.

Another important aspect of real-time implementation is having a communication channel between the upstream and the downstream station to send the signatures as they arrive. A memory buffer is also needed to store signatures before processing. Data recorded from the two channels for an hour from two lanes amounts to the size of 4,000 KB. The size of the buffer needed depends on the number of lanes of the roadway, traffic volume, and the time needed for computation. Since today's memory cost (dollar per MB) is cheap, and fast communication channels are readily available, these two issues should not present any problems in real-time implementation.

5.7 Hardware-in-Loop System

Hardware-in-Loop (HIL) systems are simulation or testing systems that include the actual hardware of the target system as a part of the simulation loop of the overall system and replaces the rest of the system with software simulation. Such a system provides a variety of lab-testing conditions without inducing risk or stress to the actual operational environment and is commonly used as a testing or development environment. In this study, an HIL system was developed for two main purposes. The first is to test the controllability and data accessibility of the Canoga card for real-time travel-time measurements. The second was to study the properties of inductance signatures under a variety of loop environments and traffic conditions under lab-bench settings.

The developed HIL system comprises loop wires embedded on a wooden board (18:1 scale), metal-cast model cars (18:1 scale), a Canoga 824T detector card, and a notebook PC that runs the simulation or testing software. The completed HIL system is shown in Figure 5.18. Since the loops embedded on a wooden board and the metal-cast vehicle models closely simulate the real road, traffic, and detector conditions, it allows a variety of tests that closely simulate the ILD environment under real traffic. Also, use of the actual detector card allows the development of software that can be used in the real system.
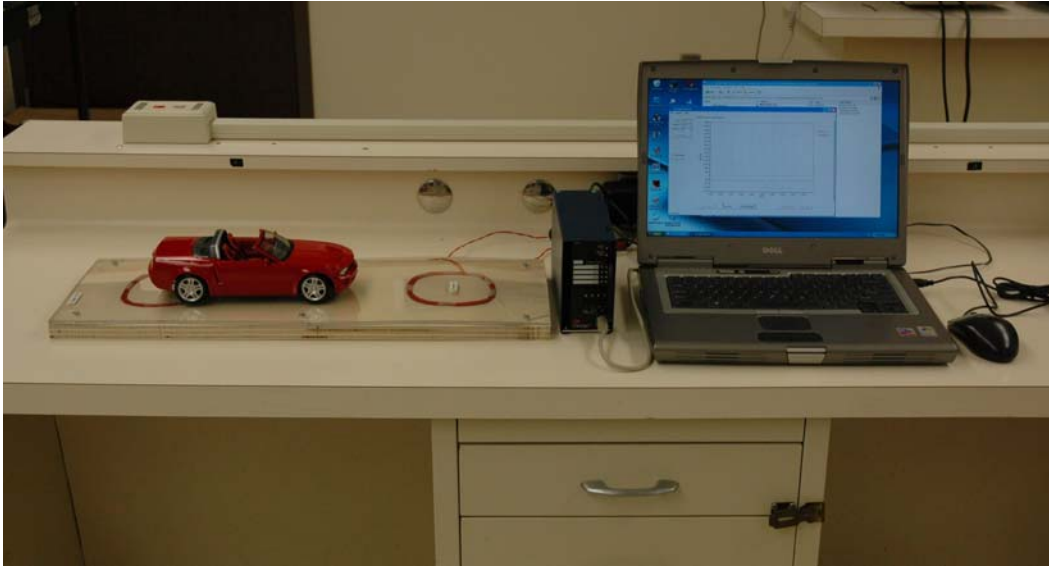
Figure 5.18: Hardware-in-Loop test system for inductance signature analysis

Software controllability of the Canoga card was tested by developing a real-time program that controls the Canoga card, reads the inductance data, stores the data in an organized file structure for later processing and plots the data in real-time. The software developed includes a basic testing utility that allows the system to send any of the available Canoga commands and to receive the responses, which enables testing of the Canoga card's properties. In the data-reading mode, it retrieves the inductance data, stores them for processing, and plots data in real-time. Further developments are still needed to function as a complete travel-time measurement unit, but all basic functions needed for travel time were implemented and tested, and it worked without any problem. Two observations to note during the software development are as follows.

- A single Canoga card is only capable of generating inductance data from two channels at a time although it contains four detector channels. This does not create any technical problems but increases the cost since each card can only be connected to two loops.

- In the inductance mode, the Canoga cards transmit inductance data without any protocol that controls the error or missing data. As a result, the computer receiving the data must have a large buffer to minimize loss of data. Also, the serial port in the

back of the card does not transmit inductance data. Hence, only the serial port in the front can be used for inductance data acquisition.

The second part of testing, to study the properties of inductance signatures under a variety of loop environments and traffic conditions under lab-bench settings, is beyond the scope of this project, but several basic conditions of traffic effects on loop inductance were tested. These tests included the effect of tail gating, lane changes, effective detection zone, and influence by surrounding environments such as stopped vehicles. The detailed results will be published in another report. Another interesting experiment done using the HIL system was to study the effect of long-loops that cover two lane widths (which are commonly used as queue detectors). For this test a long loop was created using a wooden board with 18:1 scale as shown in Figure 5.19. The question we wished to answer was whether inductance signatures are distinguishable (1) when two vehicles simultaneously pass over the loop and (2) when only a single vehicle passes over. A clear difference in the signature patterns was observed in the experiments, and it was concluded that with some signal processing the common under-counting problems in long loops can be solved. The HIL system developed allowed easy generation of such signals, and it is expected to be a useful tool for studying inductance signatures in the future.

Figure 5.19: Simulated long-loop for analysis of queue detectors

5.8 Implementation Issues

In order for the developed travel-time algorithm to be implemented in the field, three system components must be integrated. They are computational unit (computer), software, and data communication. The choices of each component are dependent on each other. For example, if a centralized collection of inductance data is chosen as the basic communication means, the computational unit in the detector cabinet needs to perform only minimal computations since it only needs to read data from the detector card and pass it to the central computer. On the other hand this scheme would require a high bandwidth in the communication channel. In order to simplify the choices, the implementation schemes are classified into centralized and decentralized, and each scheme is discussed separately.

5.8.1 Centralized implementation

Centralized implementation refers to a system in which the raw inductance data is aggregated to a central location where travel time is computed. In this case, the computer at the detector cabinet acquires the raw inductance data from the detector card, creates a compact file, and transmits it to a central location. Therefore, the computer at the detector cabinet does not need to have a high computational power, and thus single board computers (SBC) under $500 would be sufficient for this purpose. The data produced by each detector with two loops amounts to 4MB (megabytes) per hour. This is translated to 1,100 bytes per second. Assuming 5,000 detectors in the Twin Cities' freeway, it would require 5.5 MB per second or 44 Mb (megabits) per second bandwidth. Presently, RTMC uses OC3 for collecting loop detector data, which has 155 Mb per second bandwidth. Therefore, about one third of this bandwidth is needed to implement the centralized scheme. If the present OC3 network is upgraded to OC12 which has 622 Mb per second, this centralized scheme would work with sufficient room of bandwidth for future applications.

Once the inductance data is collected to a central location, a rack mounted servers could be used at the central location to compute the travel time. For a regular PC with a Pentium 4 processor, about 0.1 milliseconds of computation is needed for one second of data. A rough estimate for the number of required servers is therefore equivalent to 250

PCs of computational time. The measurement of 0.1 milliseconds is based on computation under normal operational load of PC in which other functions are concurrently working. Therefore, if the computers are dedicated to computing only travel time, the number of computers required should be significantly reduced. The amount of storage requirement for 5, 000 detectors per day is about 480 GB (gigabytes). This amounts to 175 TB (terabytes) per year, which is a fairly large amount of storage.

Centralized implementation has a benefit of having the raw data in one place from which travel-time computation could be monitored effectively from a central office. In addition, the raw data could be used for other applications such as vehicle classification. On the other hand, the cost of bandwidth, data storage, and computation are relatively high.

5.8.2 Decentralized implementation

Decentralized implementation refers to computing the travel time at the location of detector cabinets in which the raw inductance data is only transmitted to a neighboring detector station. Since the distance between two detector stations are short in Twin Cities' freeway (0.5 miles), several methods of communication channels are available. The links could be wired or wireless. Since wired links requires a high implementation cost, a more desirable choice would be wireless links.

For the computational unit, a SBC with regular PC implementation should be more than sufficient for all required computations. The raw inductance data is only required to be transmitted from the upstream station to the neighboring downstream station where travel time is computed. The computed travel time from each cabinet is then transmitted to a central location where the data is used. The amount of nonvolatile memory requirement would be dependent on how long the raw data to be kept in the local SBC. In general, the overall cost of decentralized implementation would be less than centralized implementation, while it has less control over the raw inductance data.

6. CONCLUSIONS AND FUTURE STUDY

6.1 Conclusions

This report presented study results on inductance signature restoration and its applications to vehicle re-identification. The basic signal processing technique applied was blind deconvolution, and its feature restoration capability was studied. The underlying theory was that, since many features of inductance signatures are lost by the convolution process of ILD systems, a deconvolution process (or inverse filtering) would reverse the process and restore the lost features in the inductance pattern space.

Two blind deconvolution approaches were proposed, i.e., the CLS filter and the Godard deconvolution. The CLS filter requires an estimate of loop system function, and an estimation technique based on inductance waveform analysis was proposed. Godard deconvolution is an adaptive algorithm and requires repetitive iterations until the solution converges to a local minimum. The advantage of Godard deconvolution was that it converges to a good solution even if the iteration starts from a rough or bad estimate of the ILD impulse response. However, the cost paid was a significantly higher computational time. The re-identification performance of the CLS filter was similar to that of the Godard deconvolution as long as a good estimate of the loop system function is applied.

Based on the theory and the experimental results, we confidently conclude that deconvolved signals expose significantly more unique vehicle features than the signals without deconvolution. Such signal restoration helps increase vehicle re-identification rates, which in turn increases the accuracy of travel time measurements. Therefore, we believe that the deconvolution process should be an essential part of the applications requiring inductance signature analysis. The signal processing techniques presented in this report could also be applied to other applications such as vehicle classification and tracking if they are based on inductance signature analysis.

6.2 Future Recommendations

For future study, the proposed approaches should be improved in several areas, and they are listed below.

- The computational time of the Godard deconvolution could be significantly reduced through second-order gradient-search algorithms such as a Newton algorithm, i.e., faster computational algorithms should be explored.

- Other deconvolution techniques such as an information theoretic model or higher order statistics should be tried out and compared with the techniques used in this research.

- The performance of re-identification accuracy could be further improved through utilization of a more sophisticated pattern-matching algorithm such as a dynamic time warping algorithm (Myer, et al., 1980)).

- The data set of the study should be extended to include a wide range of traffic and loop conditions to verify repeatability of the algorithm. In order to address this problem, the research team is presently in discussion with Mn/DOT on testing the algorithm on queue detection loops located near freeway ramps where vehicles wait to enter the freeway.

- Deconvolution could be used for estimating speeds from a single loop by formulating the cost function for speed estimation, i.e., the cost function is minimized when the iterated inductance signature matches with the speed. Such a technique has not been tried in the past.

- A real-time implementation should be tried on a pair of detector stations. This step would require implementation of a communication network and redesign of the algorithm steps to meet the real-time requirements.

Blind deconvolution is a well established field of signal processing. This research is the first time it has been applied to vehicle re-identification. It proved to be a powerful tool for restoring unique features of inductance signatures for vehicle re-identification. With further work and refinements as suggested above, the researcher believes that it can serve as a fundamental signal processing step for many vehicle-inductance related applications.

REFERENCES

Amari, S., A. Cichocki, and H. H. Yang, (1996), "A new algorithm for blind signal separation," *Adv. Neural Information Processing Systems*, vol. 8., pp, 757-763, 1996.

Bell, A. J., Sejnowski, T. (1995), "Blind separation and blind deconvolution: an information- theoretic approach," *Proc. ICASSP*, (Detroit), 1995.

Coifman, B. (2000), "New aggregation strategies to improve velocity estimation from single loop detectors," California PATH Paper, UCB-ITS-PWP-2000-12.

Dailey, D. (1999), "A statistical algorithm for estimating speed from single loop volume and occupancy measurement," *TRB, Vol 33B*, No 5, June 1999, pp 313-322.

Feng, C., Chi, C. (1999), "Performance of cumulant based inverse filters for blind deconvolution," *IEEE Transactions on Signal Processing*, Volume 47 Issue 7, (1922-1935), July 1999.

Godard D.N. (1980), "Self-recovering equalization and carrier tracking in a two-dimensional data communication systems," *IEEE Transactions on Communications*, Volume 28, (1867-1875), 1980.

Gonzalez, R.C., & Woods, R. E. (1993), *Digital Image Processing*, Addison-Wesley, Reading, Massachusetts, 1993.

Gray, R.M. (1990), "Entropy and information theory"
 http://www-ee.stanford.edu/~gray/it.pdf, Dec. 10, 2005.

Haykin, S. (2000), *Unsupervised adaptive filtering Volume 2: Blind deconvolution*, Wiley Inter-Science Publication, April 2000.

Johnson, R.C., Schniter, P., Endres, T.J., Behm, J.D., Brown, D.R., Casas, R.A. (1998), "Blind equalization using the constant modulus criterion: a review," *Proceedings of the IEEE*, October 1998.

Khan, S and Thanasupsin K (2000), "Estimating link travel time on I-70 corridor: a real-time demonstration prototype" by Colorado Department of Transportation, Research Branch, 4201 East Arkansas Avenue, Denver CO 80222; (http://www.dot.state.co.us, Dec. 10, 2005) [TD100:CO00-15]

Lee, W., Cheun, K. (1999), "Convergence analysis of the stop-and-go blind equalization algorithm," *IEEE Transactions on Communications*, Volume 47, No 2, February 1999.

Lucky, R.W. (1966), "Techniques for adaptive equalization of digital communication systems," *Bell System Tech. J.*, Volume 45, (255-286), 1966.

Mathis, H., Douglas S.C. (2003), "Blind deconvolution of impulsive signals using a modified Sato algorithm," *IEEE Transactions on Signal Processing*, Volume 51, Issue 7, (1905 -1915), July 2003.

Mendel, J.M. (1991), "Tutorial on higher-order statistics (spectra) in signal processing and system theory: Theoretical results and some applications," *Proceedings of the IEEE*, Volume 79, No 3, March 1991.

Mikhalkin, B., Payne, H., Isaksen, L. (1972), "Estimation of speed from presence detectors," *Highway Research Record 388*, pp 73-83. Highway Research Board, Washington, DC.

Myer, C., L.R. Rabiner, and A.E. Rosenberg (1980), "Performance tradeoffs in dynamic time warping algorithms for isolated word recognition," *IEEE Trans. Acoust. Speech Signal Processing*, vol. ASSP-28, Dec 1980, pp. 623-635.

Nokas, G., Dermatas, E., Kokkinakis, G. (1998), "Robust speech recognition in noisy reverberant rooms," Workshop on text, speech and dialogue Pilsen, Czech Republic, September, 1998.

Nowlan, S.J., & Hinton, G.E. (1993), "A soft decision-directed LMS algorithm for blind equalization," *IEEE Transactions on Communications*, Volume 41, No 2, Feb1993.

Olofosson, T., Stepinski, T. (1996), "Blind deconvolution through parametric identification using second and fourth order cummulants," Ultrasonics Symposium, 1996. *Proceedings of the IEEE*, Volume 1, (717 –721), November 1996.

Pushkar, A., Hall, F., Acha-Daza, J. (1994), "Estimation of speeds from single-loop freeway flow and occupancy data using cusp catastrophe theory model," *Transportation Research Record 1457*, pp 149-157. Transportation Research Board, Washington, DC.

Sato, Y. (1975), "Two extensional applications of the zero-forcing equalization method," *IEEE Transactions on Communications*, Volume 42, (684-687), 1975.

Shalvi, O., Weinstein, E. (1990), "New criteria for blind deconvolution of nonminimum phase systems (channels)," *IEEE Transactions on Information Theory*, Volume 36, (312-321), March 1990.

Sun, C., Ritchie, S.G. (1999), "Individual vehicle speed estimation using single loop inductive waveforms," California PATH Working Paper, October 1999.

Sun, C. (2000), "An investigation in the use of inductive loop signatures for vehicle classification," *California PATH Research Report*, March 2000.

Sun, C., Ritchie, S.G., Park, S., Oh, C. (2002)," Field investigation of advanced vehicle reidentification techniques and detector technologies – Phase 1," California PATH Research Report, March 2002.

Tam, R. (1999/2000), "PATH ATMIS: state of research annual report," California PATH Paper, UCB-ITS-PWP-2000-19.

Weerackody, V., Kassam, S.A. (1994), "Dual-mode type algorithms for blind equalization," *IEEE Transactions on Communications*, Volume 41, Issue 2, (22-28), Jan. 1994.

Yim. Y., Ygnace, J., Drane, C., (2000) "Travel time estimation on the San Francisco Bay area network using cellular phones as probes," California PATH Draft Report D2000-43.

Zheng, F.C., McLaughlin, S., Mulgrew, B., (1991), "Blind deconvolution algorithms based on 3rd and 4th order cummulants," *IEEE Transactions on Signal Processing*, Volume 41, Issue 2, (681 -691), February 1993.

Zervakis, M. E., & Kwon, T. M. (1992), "Robust estimation techniques in regularized image restoration," *SPIE Optical Engineering*, vol. 31, no. 10, pp. 2174-2190, Oct. 1992.